

Aus der Chirurgische Klinik
der Medizinischen Fakultät Mannheim
(Direktor: Prof. Dr. med. Christoph Reissfelder)

Influence of blue light irradiation on endothelial cells and weighted gene
co-expression network analysis in the development of abdominal aortic
aneurysm

Inauguraldissertation
zur Erlangung des medizinischen Doktorgrades (Dr. med.)
der
Medizinischen Fakultät Mannheim
der Ruprecht-Karls-Universität
zu
Heidelberg

vorgelegt von
Kejia Kan

aus
Jiangsu, China
2021

Dekan: Prof. Dr. med. Sergij Goerd
Referent: Prof. Dr. med. Nuh Rahbari

CONTENTS

Page

LIST OF ABBREVIATIONS	1
1 INTRODUCTION.....	3
1.1 Influence of blue light irradiation on endothelial cells.....	3
1.1.1 Role of endothelial cells in angiogenesis.....	3
1.1.2 Regulatory mechanisms of endothelial cells.....	4
1.1.3 Light therapy	5
1.1.4 Light-emitting diode light.....	6
1.1.5 Blue light	6
1.1.6 Aim of the study	7
1.2 Weighted gene co-expression network analysis in the development of abdominal aortic aneurysm	7
1.2.1 Background.....	7
1.2.2 Weighted gene co-expression network analysis.....	8
1.2.3 Aim of the study	9
2 MATERIALS AND METHODS	10
2.1 Influence of blue light irradiation on endothelial cells.....	10
2.1.1 Materials	10
2.1.2 Methods	13
2.1.3 Statistical analysis.....	22
2.2 Weighted gene co-expression network analysis in the development of abdominal aortic aneurysm	22
2.2.1 Materials	22
2.2.2 Methods	23
2.2.3 Statistical analysis.....	26
3 RESULTS	27
3.1 Influence of blue light irradiation on endothelial cells.....	27

3.1.1	Effect of blue light on cell viability	27
3.1.2	Effect of blue light on redox metabolism and apoptosis in cells.....	30
3.1.3	Effect of blue light on cell migration	34
3.1.4	Effect of blue light on cell angiogenesis.....	37
3.1.5	Gene expression analysis of cells with different fluences of blue light irradiation.....	38
3.1.6	Verification of genes in interested pathways with qPCR.....	45
3.2	Weighted gene co-expression network analysis in the development of abdominal aortic aneurysm	46
3.2.1	Construction of weighted gene co-expression network	46
3.2.2	Construction of module-trait relationships and detection of key modules	47
3.2.3	Functional enrichment analysis of genes in the module	48
3.2.4	Identification of hub genes in the key modules	51
3.2.5	Hub genes validation and key genes selection.....	52
3.2.6	Predication of drug-gene interaction	54
4	DISCUSSION	56
4.1	Influence of blue light irradiation on endothelial cells.....	56
4.1.1	Inhibition phase of blue light on endothelial cells.....	56
4.1.2	Mechanisms of inhibitory effect on endothelial cells after blue light irradiation.....	58
4.1.3	Promotion phase of blue light on endothelial cells.....	60
4.1.4	Mechanisms of promotion effect on endothelial cells after blue light irradiation.....	60
4.2	Weighted gene co-expression network analysis in the development of abdominal aortic aneurysm	61
4.2.1	Key modules of AAA progression	61
4.2.2	Hub genes related to AAA progression.....	62
4.2.3	Predicted drugs for AAA treatment	63
5	SUMMARY	65
5.1	Influence of blue light irradiation on endothelial cells.....	65
5.2	Weighted gene co-expression network analysis in the development of abdominal aortic aneurysm	65

6 REFERENCES	66
7 LISTS OF FIGURES AND TABLES	80
7.1 List of figures.....	80
7.2 List of tables.....	81
8 CURRICULUM VITAE	83
9 ACKNOWLEDGEMENT	85

LIST OF ABBREVIATIONS

°C	Grad Celsius
AAA	Abdominal aortic aneurysm
AHS	Amplifying hydrogel solution
cm ²	Square centimeter
DCFH-DA	Dichloro-dihydro-fluorescein diacetate
DGIdb	Drug-Gene Interaction Database
DLL4	Delta-like 4
EC	Endothelial cell
FAO	Fatty acid oxidation
FBS	Fetal bovine serum
FC	Fold change
GEO	Gene expression omnibus
GFP	Green fluorescent protein
GLS1	Glutaminase 1
GO	Gene ontology
GS	Gene significance
GSEA	Gene set enrichment analysis
HUVEC	Human umbilical vein endothelial cells
J	Joule
KEGG	Kyoto encyclopedia of genes and genomes
LED	Light-emitting diode
ME	Module eigengene
ml	Microliter

LIST OF ABRREVIATIONS

mW	Milliwatt
PBS	Phosphate-buffered saline
PDT	photodynamic therapy
PFKFB3	Phosphofructokinase-2/fructose-2,6-biophosphatase 3
PPAR- γ	Peroxisome proliferator-activated receptor- γ
qPCR	Quantitative polymerase chain reaction
RIN	RNA integrity number
RNA-seq	RNA Sequencing
ROS	Reactive oxygen species
SD	Standard deviation
UV	Ultraviolet
VEGF	Vascular endothelial growth factor
VEGFR2	Vascular endothelial growth factor receptor 2
WGCNA	Weighted gene co-expression network analysis
μ	Micro (10^{-6})

1 INTRODUCTION

This doctoral thesis includes two independent projects which are not thematically related. Therefore, all sections of this thesis have been divided into two separate independent parts.

1.1 Influence of blue light irradiation on endothelial cells

1.1.1 Role of endothelial cells in angiogenesis

Endothelial cells (ECs) are a single layer of epithelial cell lines in the basement membrane of blood vessels. They are the main mechanical vascular barrier that maintains vascular permeability through tight junctions ¹. Most importantly, ECs play a dominant role in the whole process of angiogenesis.

Angiogenesis is a complex event that new blood vessels generate from the pre-existing vasculature. Under hypoxia, injury or other conditions, it is rapidly initiated to form new blood vessels to deliver enough oxygen and nutrients to the affected sites ². The angiogenic process consists of the following steps: firstly, endothelial cells secrete proteolytic enzymes under external stimulations such as pro-angiogenic factors ³. These enzymes could degrade the vascular basement membrane, which paves the way for the migration of ECs through the basement membrane to the perivascular matrix ³. After the migration, these ECs proliferate and adhere to each other around the perivascular matrix to form the hollow tubular structures ⁴. Then the perivascular matrix undergoes remodeling and the ECs are surrounded by vascular smooth muscle cells and pericytes ⁵. Finally, avascular anastomosis is formed with the newly formed vascular networks. Thus, this well-regulated process of angiogenesis is highly dependent on the proliferation, migration and remodeling of ECs. The dysregulation of angiogenesis, caused by abnormal states of endothelial cells, was found in a wide range of pathological processes, including atherosclerosis, diabetes, tumorigenesis, neovascular eye diseases and so on ⁶.

1.1.2 Regulatory mechanisms of endothelial cells

1.1.2.1 VEGF signaling

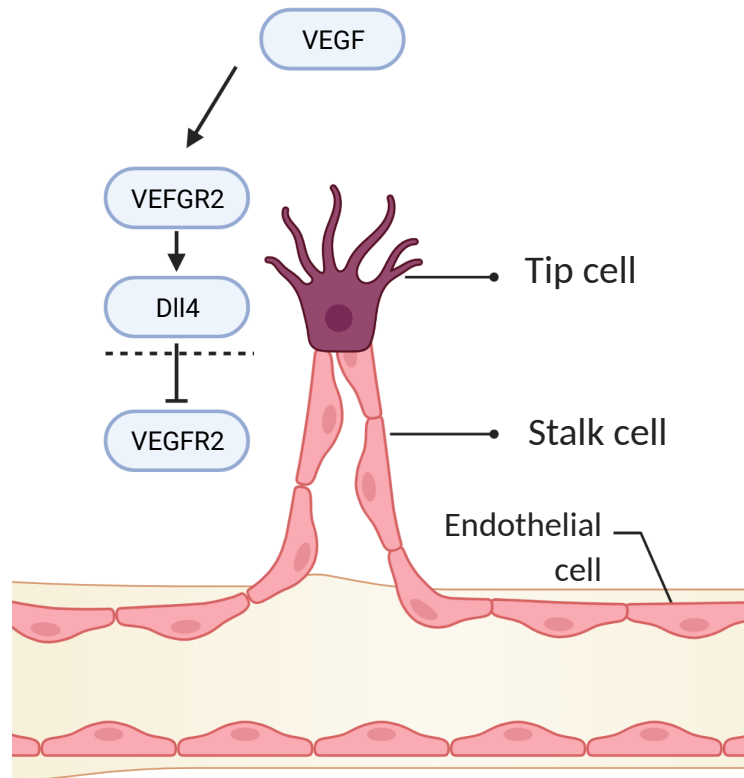


Figure 1. Molecular mechanisms of VEGF signaling in endothelial tip-stalk switch during angiogenesis. Modified from Herbert & Stainier, 2011.

During angiogenesis, endothelial cells are regulated by various signaling pathways, among which vascular endothelial growth factor (VEGF) signaling is the most important and widely studied. Vascular endothelial growth factor receptor 2 (VEGFR2) is the primary angiogenic signal-receiving receptor ⁷. VEGF could also bind to this receptor inducing the switch of ECs from quiescent cells to tip cells, producing filopodia and guiding the following endothelial cells ⁸. After the induction, Delta-like 4 (DLL4) expressed by tip Endothelial cells dynamically compete for the tip cell position during angiogenic sprouting. Endothelial cells would downregulate the VEGFR2 expression in endothelial cells nearby and switch these cells to a more proliferated phenotype called stalk cells (**Figure 1**) ⁸. When the two adjacent tip cells contact each other, a tube-like structure will be formed. The VEGF signaling controls the tip-stalk switch process of endothelial cells during angiogenesis. Some in vivo studies

had proved the crucial role of VEGF signaling in angiogenesis and development^{9–11}. The knockout of VEGFA or VEGFR2 in the mouse embryo, a member of the vascular endothelial growth factor family, would result in fatal death due to abnormal function and development of the circulatory system^{12,13}.

1.1.2.2 Metabolism

Metabolic activities of endothelial cells support cell proliferation and migration by converting nutrients into energy and biomolecules¹⁴. Studies suggested that metabolism could also influence the endothelial cells in angiogenesis¹⁴. The energy metabolism of ECs exclusively depends on glycolysis, a process that converts glucose into pyruvate with the production of ATP. It was reported that 85% of ATP was produced by this process in ECs^{15–17}. In human umbilical vein endothelial cells (HUVECs), glycolytic flux was 200 times more than glucose oxidation¹⁸. During angiogenesis, VEGF could upregulate the expression of glucose transporter 1 (GLUT1), which promotes the uptake of glucose in ECs¹⁹. The phosphofructokinase-2/fructose-2,6-bisphosphatase 3 (PFKFB3), a key enzyme in glycolysis, was upregulated simultaneously, so the glycolysis of ECs and angiogenesis were enhanced^{18–20}. Besides the regulatory role of glucose metabolism in angiogenesis, fatty acid oxidation (FAO) was shown as the crucial effect in ECs sprouting. Carnitine palmitoyltransferase 1A (CPT1A) is a rate-limiting enzyme for FAO that regulates the transfer of fatty acids into the mitochondria for oxidation²¹. Knockdown of CPT1A in ECs would inhibit the cell proliferation and sprout of tip cells through decrease the process of FAO and production of deoxy-ribonucleoside triphosphate (dNTP)²². Amino acids are other essential nutrients for ECs. Glutamine metabolism is the most studied among amino acid metabolism in ECs angiogenesis. Glutaminase 1 (GLS1) is an enzyme that catalyzes the hydrolysis of glutamine to glutamate. One in vivo study revealed that inhibition of GLS1 attenuated the migration of tip cells and proliferation of stalk cells, which further inhibited the angiogenic process²³.

1.1.3 Light therapy

Light therapy is an emerging therapeutic approach for different kinds of diseases using daylight (visible light) and artificial light sources (infrared, ultraviolet or laser). At present, there are three main types of light therapy: photodynamic therapy (PDT), photoimmunotherapy (PIT) and photothermal therapy (PTT)²⁴. PDT and PIT are the treatments that use light to activate photosensitizer to produce reactive oxygen

species (ROS) or activate immune responses ²⁴, and PTT is defined as a method that induces cell death through local heat ²⁵.

The therapeutic effects of light therapy are based on the energy carried by light quantum, which could induce the photochemical effect and photothermal effect ²⁶. The photochemical effect is initiated from the activation of intercellular molecules which absorb the corresponding wavelength photons. During energy level transition, the above-activated molecules would further provide free radicals, which leads to the oxidation of the macromolecules such as proteins, lipids and DNA ²⁶.

1.1.4 Light-emitting diode light

Light-emitting diode (LED) is a new semiconductor device that can provide emission wavelengths from 380 nm to 760 nm. It has the following advantages: It is small, light and durable from its physical characteristics; It provides a cold light with efficient energy transformation; Last but not least, it is the most mature device with high brightness, low energy consumption and long lifetime ²⁷. Nowadays, LEDs are widely used in biomedicine including medical lighting, diagnosis and treatment ²⁸.

1.1.5 Blue light

Blue light is one component of visible light with wavelength ranges from 380 nm to 500 nm. Due to its high energy, blue light has displayed bactericidal potency similar to UV light ²⁹. Moreover, blue light is also known for its anti-inflammatory properties, which are helpful for the treatment of inflammatory-related diseases such as acne vulgaris ^{30,31} and psoriasis ³². Other conditions like neonatal jaundice ³³ and local pain ³⁴ are also treated with blue light.

The best-known clinical application of blue light is in the treatment of neonatal jaundice caused by excess bilirubin in the blood, a common physiological condition that affects 60-70% of newborns worldwide ³⁵. Due to the simple and effective way with minor side effects of blue light irradiation, it is the preferred method for treating neonatal jaundice ³⁶. The bilirubin in the skin after blue light (460 nm) irradiation would change into a water-soluble isoform which could be excreted through body fluids, feces and urine ³⁶. The treatment of plaque-induced gingivitis is another application of blue light. By activating porphyrin in bacterial, blue light (405-420 nm) could induce oxidative stress damage, including lipid and protein oxidation, oxidative damage to DNA, which further inhibits bacterial growth ³⁷.

The potential application of blue light in angiogenesis was revealed by several *in vivo* studies. One animal study showed that blue light (470 nm) could increase angiogenesis and promote wound healing in an ischemia rodent flap model. The ischemic tissue necrosis was reduced, and flaps showed significantly increased tissue perfusion at day 7 in the blue LED-treated group ³⁸. Another clinical study showed that blue light exposure (453 nm) could decrease blood pressure by increasing circulating nitric oxide thereby improving the EC function ³⁹.

Contradictory, one study showed that blue light (475 nm) did not affect the migration of ECs or vasculogenesis ⁴⁰, and it may inhibit the growth of aortic endothelial cells *in vitro* ⁴¹.

1.1.6 Aim of the study

This study aimed to detect the effect of blue light irradiation on endothelial cells *in vitro*. The first step is to know the influence of irradiation parameters (time and irradiance) of blue light on cells. After the parameter's settings have been defined, endothelial-specific cell functions, including migration, tube formation and sprouting will be tested after blue light treatment, as they are essential functions for angiogenesis.

Key questions of the project are:

1. What are the responses of blue light on endothelial cells when applying different irradiation parameters including irradiance and time?
2. Does blue light affect the angiogenesis-related function of endothelial cells? Promotion or Inhibition?
3. How does blue light affect the angiogenic functions *in vitro*? Which genes or pathways may involve in this regulation?

1.2 Weighted gene co-expression network analysis in the development of abdominal aortic aneurysm

The present work was published in *Biomedicines* 2021, 9(5), 546; <https://doi.org/10.3390/biomedicines9050546>.

1.2.1 Background

Abdominal aortic aneurysm (AAA) is a common aortic disease characterized by a localized dilation or bulging of the abdominal aorta ⁴². Without treatment it causes high mortality among the aged as most AAA patients remain asymptomatic for years

or even decades. It is estimated that around 200,000 AAA rupture cases are diagnosed worldwide annually. The overall mortality after rupture remains approximately 80%^{43–45}.

Currently, the indications of AAA treatment are large aneurysms with a diameter of more than 5.5 cm⁴⁶, and aneurysms that expand rapidly in a short period or compromise the perfusion to distant organs. Open surgical repair (OSR) or endovascular aortic repair (EVAR) is the only possible measures that provide a definite treatment. In OSR, patients carry higher perioperative risk and longer hospital length of stay^{47,48(pp1995–2008)} while EVAR may have high reintervention rates because of endoleaks, graft migration which all may lead to secondary rupture^{49,50}. For patients with small AAAs or those who are not eligible for AAA repair, available treatment approaches are limited to close aneurysm surveillance and adjuvant medical therapy⁵¹. So far, no effective pharmacological treatments have been developed to prevent AAA growth or rupture^{52,53}. Hence, there is a need to elucidate the possible mechanisms of AAA progression and explore complementary pharmaceutical treatments.

The molecular mechanisms of AAA pathogenesis are not fully known. Several studies based on the high-throughput microarray profiling indicated that many biological processes such as immune response, chronic inflammation, and reactive oxygen species might be involved^{54–56}. Dozens of genes related to AAA development were identified through gene expression profiles^{57–59}. However, these studies exclusively focused on the differentially expressed genes (DEGs) between AAA and control groups, which ignored some essential genes highly correlated to specific sample traits of AAA.

1.2.2 Weighted gene co-expression network analysis

Weighted gene co-expression network analysis (WGCNA) is a bioinformatics algorithm developed by Horvath et al.⁶⁰. It is a systematic biological method that describes the gene co-expression pattern between different samples. By constructing a scale-free weighted network, it can be used to identify gene sets and the candidate biomarkers or targets of the disease based on the connectivity between gene modules and sample traits (**Figure 2**). Compared to the traditional differential gene expression analyses, which so far focused on genes characterizing the difference between groups, WGCNA, groups co-expressed genes in an unbiased manner into modules in which genes are highly related to each other, and these modules could

be further connected to the external information, such as sample characteristics. WGCNA has been successfully used to identify key modules and hub genes related to cardiovascular diseases, such as atherosclerosis, heart failure, and acute myocardial infarction ^{61–63}.

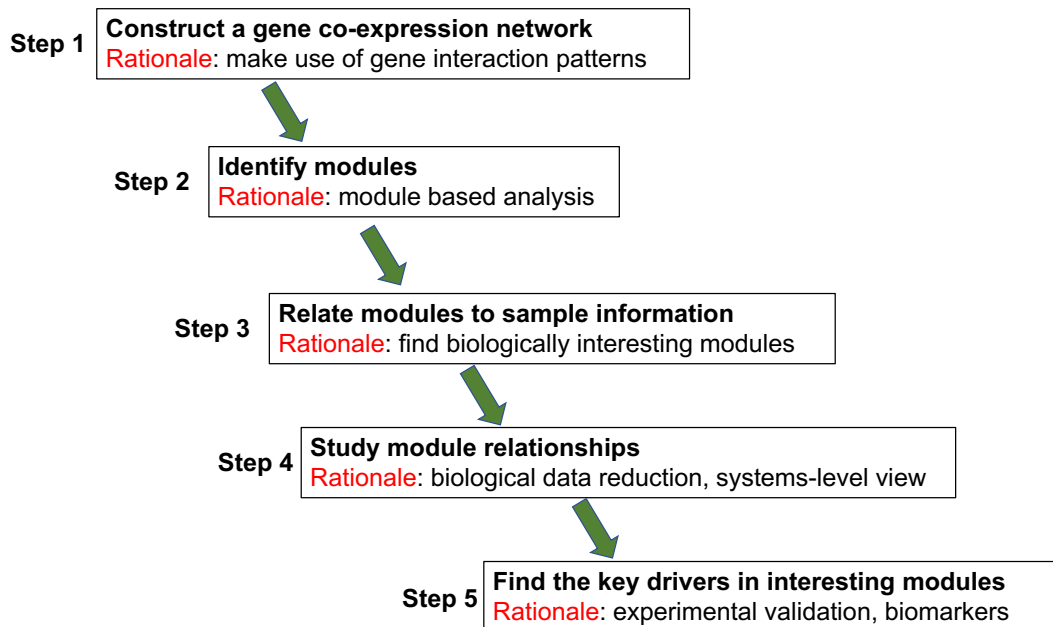


Figure 2. A brief overview of weighted gene co-expression network analysis (according to Langfelder and Horvath 2008).

1.2.3 Aim of the study

The aim of this project was to bioinformatically explore the underlying molecular mechanisms of abdominal aortic aneurysm (AAA) progression and to identify potential drugs targeting the key genes involved in the growth. We base this analysis on data available from public datasets related to AAA and weighted gene co-expression network analysis (WGCNA). Accordingly, the following questions were issued in this project:

1. How were the genes clustered (gene modules) in AAA progression through WGCNA analysis?
2. What were the biological functions of key modules involved in AAA growth?
3. Which genes in the key modules are the key players in AAA progression and could be used as drug targets?
4. What compounds or drugs may be potentially used to limit the AAA growth based on the drug-gene prediction?

2 MATERIALS AND METHODS

2.1 Influence of blue light irradiation on endothelial cells

2.1.1 Materials

2.1.1.1 Blue light device

The blue light LED device is a wearable medical device provided by URGO RID (URGO RID, Chenôve, France). It was used in the European project MEDILIGHT (**Figure 3**). A mobile software (URGO RID, Chenôve, France) was developed to control the device via Bluetooth.



Figure 3. The blue light device from the top side (left) and the bottom side (right).

2.1.1.2 Consumables

Name	Manufacturer
Cell culture plate, 96-well black plate	Corning, Kennebunk, ME, USA
Cell culture flasks, different sizes	Greiner Bio-One, Frickenhausen, Germany
Cell culture plate 6-well, transparent	Greiner Bio-One, Frickenhausen, Germany
Cell culture plate 12-well, transparent	Greiner Bio-One, Frickenhausen, Germany
Cell culture plate 12-well, black	In vitro Scientific, Mountain View, CA
Cell culture dish, 10 cm	Greiner Bio-One, Frickenhausen, Germany
Cell Culture Inserts in Multi-Well Plates (8 µm)	Thermo Fisher Scientific, Roskilde, Denmark

Name	Manufacturer
Cryotube Vials	Thermo Fisher Scientific, Roskilde, Denmark
Falcon tube (15 ml, 50 ml)	Greiner Bio-One, Frickenhausen, Germany
LightCycler 480 Multiwell Plate 96, white	Roche Diagnostics, Mannheim, Germany
Pipette tips, with filter (10 µl, 100 µl, 1 ml)	Eppendorf AG, Hamburg, Germany
Serological pipettes (5 ml, 10 ml, 20 ml)	Greiner Bio-One, Frickenhausen, Germany
µ-Slide angiogenesis	ibidi GmbH, Munich, Germany
Vivaspin 500 centrifugal filter	Sartorius, Goettingen, Germany

2.1.1.3 Chemicals and reagents

Name	Manufacturer
Acrylamide, 2x cryst	Carl Roth, Karlsruhe, Germany
AllPrep DNA/RNA/Protein Mini Kit	Qiagen, Hilden, Germany
BrdU Cell Proliferation ELISA Kit (colorimetric)	Roche Diagnostics GmbH, Roche Applied Science, Mannheim, Germany
Collagen I, Rat Tail	Corning, NY, USA
Colorimetric Cell Viability Kit III (XTT)	PromoCell, Heidelberg, Germany
Crystal violet	Carl Roth, Karlsruhe, Germany
Dimethyl Sulfoxide (DMSO)	Sigma-Aldrich, Munich, Germany
Endothelial cell growth medium	Provitro, Berlin, Germany
FastStart Essential DNA Green Master	Roche, Basel, Switzerland
FBS, Qualified, HI	Gibco by Thermo Fisher Scientific, Waltham, MA, USA
Gelatin from bovine skin	Sigma-Aldrich, Munich, Germany

Name	Manufacturer
Matrigel Basement Membrane Matrix	Corning, NY, USA
METAFFECTENE	Biontex Laboratories, München, German
Methylcellulose	Sigma-Aldrich, Munich, Germany
N,N'-Methylene bisacrylamide	Carl Roth, Karlsruhe, Germany
Penicillin-streptomycin	Sigma-Aldrich, Munich, Germany
Phosphate buffered saline (DPBS)	Gibco by Thermo Fisher Scientific, Waltham, MA, USA
QuantiTect Primer	Qiagen, Hilden, Germany
QuantiTect Reverse Transcription Kit	Qiagen, Hilden, Germany
ROTI Stock 10x PBS	Carl Roth, Karlsruhe, Germany
Sodium acrylate	Carl Roth, Karlsruhe, Germany
Sodium formaldehyde sulfoxylate	Carl Roth, Karlsruhe, Germany
VA-044	BIO-RAD, Munich, Germany

2.1.1.4 Instruments

Name	Manufacturer
Cell incubator, Galaxy 170 S	Eppendorf, Hamburg, Germany
Agilent 2100 Bioanalyzer	Agilent Technologies, Santa Clara, CA, USA
Centrifuge, 5920R	Eppendorf, Hamburg, Germany
HERA freeze	Thermo Fisher Scientific, MA, USA
Inverted Microscope DM IRB	Leica Mikroskopie & Systeme, Wetzlar, Germany
Laboratory vacuum pumps	Integra Biosciences, Chur, Switzerland
LightCycle®96 PCR Detection System	Roche, Basel, Switzerland
LUNA Automated Cell Counter	Logos Biosystems, Villeneuve d'Ascq, France

Name	Manufacturer
Microscope, Axio200M	Carl Zeiss Microscopy, Göttingen, Germany
Power meter 843-R-USB	Newport, Irvine, Canada
Safe 2020 Class II Biological Safety Cabinets	Thermo Fisher Scientific, MA, USA
SP8 confocal Microscope	Leica Mikroskopie & Systeme, Wetzlar, Germany
Spark Multimode Microplate reader	Tecan, Männedorf, Switzerland
T100 Thermal Cycler	Bio-Rad, Hercules, USA
Water bath, TSGP15D	Thermo Fisher Scientific, MA, USA

2.1.1.5 Software

Name	Manufacturer
ImageJ	NIH Image, NIH Bethesda, USA
AutoScratchSeg	MATLAB, Mathworks, MA, USA
AutoWoundSeg	MATLAB, Mathworks, MA, USA
GraphPad Prism 8	Graphpad Prism Software, San Diego, USA
Leica Application Suite X (LAS X)	Leica, Wetzlar, Germany
LightCycler 96	Roche, Mannheim, Germany
MEDILIGHT App V2.5	Urgo, Chenôve, France
R Studio	R Studio, Boston, MA, USA
SparkControl	Tecan, Grödig, Austria
SPSS 19.0	IBM, NY, USA
ZEN 2 (blue edition) Axio Scan software	Carl Zeiss, Oberkochen, Germany

2.1.2 Methods

2.1.2.1 Human umbilical vein endothelial cells: isolation and cell culture

Human umbilical vein endothelial cells (HUVECs) were isolated from fresh umbilical cords using the methods described by Jaffe et al. ⁶⁵. Umbilical cords were obtained

from donors from Gynecology and Obstetrics department. HUVEC isolation was approved by the local ethics committee (Medizinische Ethik-Kommission II, Medizinische Fakultät Mannheim, 2015-581N-MA). Endothelial cells were isolated from human umbilical veins by digestion with 1% collagenase V for 8 min at 37°C. After that, the vein was flushed with sterile endothelial cell growth medium to collect the endothelial cells. The cells were maintained in the 25 cm² flask pre-coated with 1% gelatin at 37°C under 5% CO₂. The cell culture medium consisted of endothelial cell growth medium (Provitro, Berlin, Germany) supplemented with 5% FBS, endothelial cell growth supplement mix (Provitro, Berlin, Germany) and 1% antibiotics (100 units/ml penicillin-streptomycin). Cells from three donors were pooled together to avoid a batch effect. HUVECs from passages two to five were used for further experiments.

2.1.2.2 Blue light irradiation

2.1.2.2.1 Irradiation dose measurement



Figure 4. Schematic diagram of blue light power measurements.

To measure the power density received by the cells, the Power Meter 843-R-USB from Newport Corporation (Newport, Irvine, Canada) was used to quantify the irradiation energy (**Figure 4**). The total doses of blue light irradiation, which were tested in this study, are listed in **Table 1**.

Table 1. Irradiation parameters were used in the study.

Irradiance (mW/cm²)	Time (minute)	Fluence (J/cm²)
10	7, 12, 15, 20, 30, 60, 90, 120	4.2, 7.2, 9, 12, 18, 36, 54, 72
20	7, 12, 15, 20, 30, 60, 90, 120	8.4, 14.4, 18, 24, 36, 72, 108, 144
5, 7.5, 10, 15, 20, 25, 40	12	3.6, 5.4, 7.2, 10.8, 14.4, 18, 28.8

2.1.2.2.2 Blue Light treatment

30 minutes before irradiation, the cell culture medium was changed to provide optimal nutrition to the cells. Then, HUVECs were treated with different doses of blue light irradiation as planned. All the experiments were performed inside the cell culture incubator (37°C, 5% CO₂). To avoid any scattering of light, plates with black bottoms were used, and the right side of the black plates was covered with aluminum foil (**Figure 5**) during irradiation. A cycling irradiation mode of 30 seconds on and 30 seconds off was used to avoid overheating.

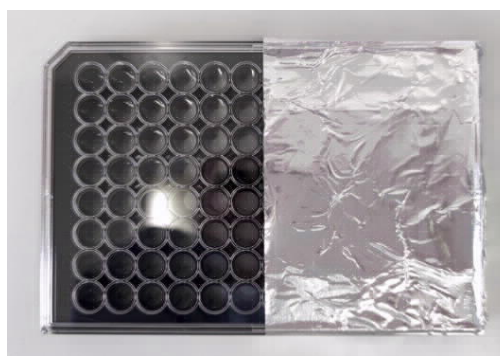


Figure 5. Schematic diagram of black plates used for the experiments. The left area was used for irradiation and the right side covered with aluminum foil was used as the control group without light illumination.

2.1.2.3 Cell viability assay

Cell viability assay was tested using the Colorimetric Cell Viability Kit III (XTT) (PromoCell, Heidelberg, Germany) to examine the effect of blue light on HUVECs. HUVECs were seeded in 96-well black plates (10,000 cells/well) and cultured until

adherence. Later cells were irradiated accordingly and cells were cultured overnight. Then 50 μ L of reaction reagent was added to each well and incubated for 30 minutes. The absorbance was measured using a microplate reader (Tecan, Männedorf, Switzerland) at a wavelength of 490 nm and a reference wavelength of 650 nm. Results were normalized with non-irradiated controls.

2.1.2.4 Cell proliferation assay

To confirm the effect of blue light on cell proliferation, the colorimetric ELISA-BrdU kit (Sigma-Aldrich, Munich, Germany) was used for this assay. 10,000 cells/well of HUVECs were seeded in 96-well black plates and cultured until adherence. Later blue light irradiation was performed accordingly and cells were cultured overnight. Then 10 μ L of BrdU label solution was added to each well and cells were incubated for 3 hours. After incubation, the medium was removed and the cells were fixed by adding FixDenat. Next, the cells were incubated with the anti-BrdU-peroxidase (POD) antibody for 90 minutes at room temperature. After the removal of excess anti-BrdU-POD antibody, the cells were washed and the substrate solution was added. Then the absorbance was measured using a microplate reader (Tecan, Männedorf, Switzerland) at the wavelength of 450 nm and a reference wavelength of 630 nm. Results were normalized with the non-irradiated control group.

2.1.2.5 Reactive oxygen species measurement

Two approaches were used to measure the change in intracellular reactive oxygen species (ROS) after blue light irradiation.

2.1.2.5.1 Transduction with the redox sensor

Grx1-roGFP3, a ratiometric fluorescence sensor, could dynamically track the glutathione redox potential with high sensitivity and temporal resolution⁶⁶. The ratio of emission intensities following excitation at 395 and 485 nm indicates the degree of sensor oxidation; a higher ratio corresponds to a more oxidized state of glutathione in cells (**Figure 6**).

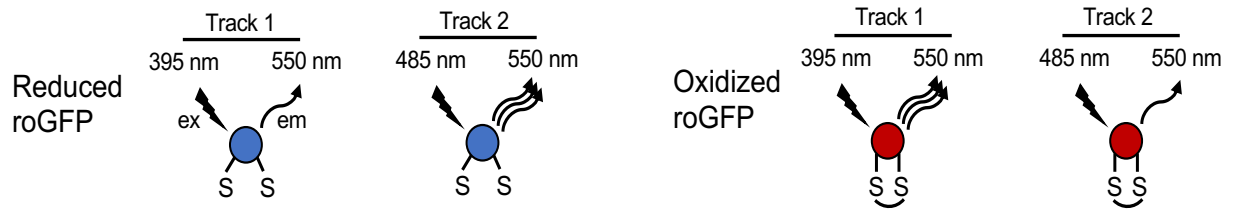


Figure 6. The principle of the assay using Grx1-roGFP3. Modified from Gutscher et al., 2008.

This sequence of sensor (kindly provided from Dr. Manfred Frey, Steinbeis-Innovationszentrum Zellkulturtechnik, University of Applied Sciences, Mannheim) was synthesized by Genewitz (ID: B32523-1/q28382) with BamHI and XbaI restriction sites and cloned into SIN lentivirus vector pHR'SIN-cPPT-SEW⁶⁷.

Lentivirus was produced using the methods described by Demaison C et al.⁶⁷. HEK293T/17 cells were transiently transfected with plasmid pHR'SIN-roGFP3, pCMV8.91, and pMD.G using transfection reagent METAFECTENE (Biontex Laboratories, München, Germany). After 48 hours, cell supernatant was collected with a centrifugal filter (Vivaspin 500, MWCO 100,000; Sartorius, Goettingen, Germany). The concentrated supernatant was aliquoted and stored at -80°C.

HUVECs were transduced with the above lentivirus for 48 hours. The transduced GFP-positive HUVECs were sorted using a BD FACSAria IIu (Becton Dickinson, Heidelberg, Germany) and used for further experiments.

2.1.2.5.2 Measurement using the redox sensor

HUVECs transduced with the lentiviral Grx1-roGFP3 sensor were seeded in 96-well plates at the concentration of 10,000 cells/well until adherence. Cells were treated with blue light accordingly. The fluorescence irradiance in each well was detected at an excitation wavelength of 395 nm and 485 nm and an emission wavelength of 550 nm by using a microplate reader (Tecan, Männedorf, Switzerland). The fluorescence ratio 395/485 nm was shown as the results.

2.1.2.5.3 Measurement using the DCFH-DA dye

The production of intracellular ROS was also determined using DCFH-DA as the fluorescent probe (Sigma-Aldrich, Munich, Germany). HUVECs (10,000 cells/well) were seeded in 96-well plates and cultured for 24h until adherence. After blue light

irradiation, the culture supernatant was removed and washed with phosphate-buffered saline (PBS). Then the cells were stained with 10 μ M DCFH-DA in a serum-free medium for 30 min in the dark. After that, cells were washed three times with PBS. The fluorescence intensity was detected at an excitation wavelength of 488 nm and an emission wavelength of 525 nm using a microplate reader (Tecan, Männedorf, Switzerland). Final results were shown as the percentage compared to non-irradiated cells.

2.1.2.6 Migration assay

To determine the migration activity of HUVECs after blue light irradiation, the migration assay was performed by using two methods: the scratch wound assay and the trans-well assay.

2.1.2.6.1 Scratch assay

1×10^6 cells/well HUVECs were grown to 90% confluence on six-well plates. Cells were starved for 2 hours before the experiment. Cells were then scratch-wounded using a sterile 20- μ L pipette tip and washed twice with phosphate-buffered saline (PBS) to remove cell debris and cultured with a complete medium. Then cells were treated with blue light accordingly. The images were taken at different time points (0, 0.4, 6, 9 and 12 h) and analyzed with ImageJ software (NIH Image, NIH Bethesda, USA). Wound closure was determined by the equation as follows:

Wound closure (%) = (Original wound area - area at each time point)/Original wound area.

2.1.2.6.2 Trans-well assay

For the trans-well assay, 24-well trans-well plates with polycarbonate membrane filters containing 8 μ m pores (Corning, New York, USA) were used. 500 μ L normal cell culture medium was added into the lower chamber and cells were seeded on the inserts pre-coated with 1% gelatin at a concentration of 8×10^4 cells/well. Then cells were treated with blue light. After 6 hours, the cells in inserts were fixed with 4% paraformaldehyde for 30 minutes and then cells were washed with PBS two times and stained with 0.1% Crystal violet for 30 minutes. Later, non-migrating cells were removed with cotton swabs from the upper surface of the membrane. Five representative fields were randomly chosen and the numbers of penetrated cells were counted using ImageJ software (NIH Image, NIH Bethesda, USA).

2.1.2.7 Angiogenesis assay

The angiogenesis ability of HUVECs after blue light treatment was investigated using two methods: the tube formation assay and the spheroids sprouting assay.

2.1.2.7.1 Tube formation assay

30 μ l Matrigel (Corning, NY, USA) was added into 15-well μ -angiogenesis slides (ibidi GmbH, Munich, Germany) and then incubated at 37 °C with 5% CO₂ for 30 minutes to polymerize the Matrigel. HUVECs were seeded onto the Matrigel layer at a density of 5,000 cells/well. Then cells were treated with blue light accordingly. After 6 hours, tubular structures of endothelial cells were photo-documented using an inverted microscope (Leica Mikroskopie & Systeme, Wetzlar, Germany) and quantified with ImageJ software (NIH Image, NIH Bethesda, USA).

2.1.2.7.2 Spheroids sprout assay

2.1.2.7.2.1 Spheroids generation

GFP-positive HUVECs spheroids were prepared using the hanging drop method⁶⁸. 800 cells/25 μ l of cell drops were dispensed on the inner side of a 10-cm dish lid. The dish was carefully inverted and kept in the cell culture incubator at 37 °C and 5% CO₂. The droplets were allowed to form spheroids overnight.

2.1.2.7.2.2 Spheroid sprouting induction

The HUVEC spheroids were collected using a 10 ml pipette to wash off the droplets with 10 ml PBS gently. Then spheroids were spun down at 200g for 5min and suspended in collagen medium containing 5 μ g/ml collagen from rat tail, serum-free medium with 20% methylcellulose (Sigma-Aldrich, Munich, Germany). The spheroid-collagen solution was added into the 15-well μ -angiogenesis slides (ibidi GmbH, Munich, Germany) and incubated in the cell culture incubator at 37 °C and 5% CO₂ for 30 min to allow collagen matrix polymerization. Then cells were treated with blue light accordingly. After 8h, the sprouting was stopped by adding the amplifying hydrogel solution (AHS). The slides were stored at 4 °C overnight. **Table 2** shows the AHS composition.

Table 2. Preparation of the amplifying hydrogel solution (AHS).

Solution components	Concentration	Manufacturer
40% acrylamide	20%	Bio-Rad, Munich, Germany
2% bis-acrylamide	0.05%	Bio-Rad, Munich, Germany
16% PFA	4%	Electron Microscopy Sciences, Hatfield, USA
Sodium acrylate	10%	Sigma-Aldrich, Munich, Germany
10% VA-044	0.1%	FUJIFILM, Osaka, Japan
10× PBS	1×	Sigma-Aldrich, Munich, Germany

2.1.2.7.2.3 Spheroid sprouting imaging

The next day, μ -angiogenesis slides were incubated in a humidified chamber at 37 °C for 2 hours until the AHS solution polymerized. To avoid oxidation, the AHS solution was sealed with parafilm. Later, the spheroids-containing gel was taken out for imaging. The samples were imaged on a Leica SP8 laser confocal fluorescence microscope (Leica Mikroskopie & Systeme, Wetzlar, Germany) with the excitation wavelength at 488 nm and emission wavelength at 509 nm. The results were quantified with ImageJ software (NIH Image, NIH Bethesda, USA).

2.1.2.8 RNA isolation

Total RNA was extracted using AllPrep DNA/RNA/Protein Mini Kit (Qiagen, Hilden, Germany) according to the manufacturer's instructions. After irradiation with different doses of blue light, cells were lysed with 600 μ l of RLT lysis buffer for 5 minutes. Lysates of cells were transferred to the DNA spin column tube and centrifuged at 8000 g, 4°C for 30 seconds then equal volumes of 70% ethanol were added to the flow-through. 700 μ l of the liquid was transferred to the RNeasy spin column and centrifuged at 8000 g, 4°C for 30 seconds. Later the RNeasy spin column was washed by RW1, RPE successively. The RNA was dissolved by adding 30 μ l of RNase-free water to the RNeasy spin column and kept at -80°C.

2.1.2.9 RNA quantification and quality control

The isolated RNA was quantified using the Spark microplate reader (Tecan, Männedorf, Switzerland). RNA purity was evaluated by the absorbance ratio at

A260/280 with acceptable values of 1.8-2.1. To determine the RNA quality, the Agilent 2100 Bioanalyzer and the RNA 6000 Nano Kit (Agilent, Waldbronn) were used. The procedure was done according to the manufacturer's instructions. The results were analyzed with the Agilent 2100 Bioanalyzer and the RNA integrity number (RIN) was calculated by Agilent software. The RIN ranges from 1 to 10, high RIN values indicate intact and pure RNA samples.

2.1.2.10 RNA sequencing

For RNA sequencing, three RNA samples of each group were analyzed with the BGISEQ-500 method. This work was done by BGI Tech Solutions Co. (Hong Kong, China).

2.1.2.11 Bioinformatic analysis of RNA sequencing

To analyze the RNA sequencing data, the R software (version 3.6.3) and NGS analysis R package systempipeR (version 1.22.0) were used. Quality control and adapter trimming of raw data were performed using FastQC (version 0.11.5) and Trim-galore (version 0.4.1) (www.bioinformatics.babraham.ac.uk). Then the resulting reads were aligned to the reference human genome, GRCh38.p13, and counted using Kallisto (version 0.46.1). The count data were transformed to log₂-counts per million (logCPM) with the limma package (version 3.44.3). Differential gene expression analysis was performed by the DESeq2 package (version 1.28.1). Gene enrichment analysis was made with fgsea package (version 1.14.0) and the EnrichmentBrowser package (version 2.18.1) using the public pathway database KEGG (<https://www.genome.jp/kegg/pathway.html>).

2.1.2.12 qPCR validation

Total RNA was isolated as described above. cDNA was synthesized by reverse transcription of the total 500 ng RNA with Reverse Transcription Kit (Qiagen, USA). All Primers were purchased as DNA Oligo-Primer from Qiagen. Real-time PCR was performed on a Roche LightCycler480 Real-Time PCR System. The relative amount of each mRNA was calculated using the $2^{-\Delta\Delta Ct}$, which $\Delta\Delta Ct = \Delta Ct$ "treatment" - ΔCt "control." The information of all primers used in this study is listed in **Table 3**.

Table 3. Information of primer used in the study.

Gene Symbol	Qiagen category number
VEGFA	QT01010184
KDR	QT00069818
NOS3	QT00089033
PLA2G4A	QT00085813
PTGS2	QT00040586
CDKN1A	QT00044233
TP53	QT02377634
CDK2AP1	QT00226198
CASP9	QT00036267
BAX	QT00031192
GAPDH	QT01192646

2.1.3 Statistical analysis

Statistical analyses were performed using Graphpad Prism. Variables were summarized as mean \pm standard deviation (SD). The unpaired Student's t-test was used to determine statistical significances between two groups. The number of technical and experimental replicates can be found in the figure legends for each experiment. *P* values less than 0.05 were considered significant and represented graphically as *, *P*<0.05; **, *P*<0.01; ***, *P*<0.001, unless otherwise indicated.

2.2 Weighted gene co-expression network analysis in the development of abdominal aortic aneurysm

The present work was published in *Biomedicines* 2021, 9(5), 546; <https://doi.org/10.3390/biomedicines9050546>.

2.2.1 Materials

2.2.1.1 Software

Name	Version	Access
R	3.6.3	https://www.r-project.org
R studio	1.4.1023	https://rstudio.com
Cytoscape	3.8.2	https://cytoscape.org
cytoHubba	0.1	http://apps.cytoscape.org

2.2.1.2 R package

Name	Version	Access
sva	3.12	https://bioconductor.org
limma	3.38.3	https://bioconductor.org
WGCNA	1.69	https://cran.r-project.org
ggcorrplot	0.1.3	https://cran.r-project.org
clusterProfiler	3.10	https://bioconductor.org
ggalluvial	0.11.1	https://cran.r-project.org
ggplot2	3.2.1	https://cran.r-project.org

2.2.1.3 Data source

GSE Dataset	Platform	Organism	Sample number
GSE17901	GPL4134	Mouse	AAA day7: 7, AAA day14: 5, AAA day28: 6
GSE12591	GPL7215	Mouse	Control: 6, AAA: 5
GSE7084	GPL 570	Human	Donor: 10, AAA: 9
GSE47472	GPL 10558	Human	Donor: 8, AAA: 14
GSE57691	GPL 10558	Human	Donor: 10, AAA: 49

2.2.2 Methods

2.2.2.1 Data sources and data preparation

We performed a systematic search in the gene expression omnibus (GEO) database (<https://www.ncbi.nlm.nih.gov/geo/>) to find the abdominal aortic aneurysm (AAA) associated gene expression datasets. Datasets GSE17901, GSE12591, GSE7084, GSE4742 and GSE57691 were downloaded and used for further analysis. The whole workflow of this study was shown in **Figure 7**. In the explore dataset GSE17901, mouse aneurysmal aortic samples consisting of the entire suprarenal aorta were taken on day 7, day 14, and day 28 from ApoE^{-/-} mice treated by angiotensin II or saline⁵⁹. Gene expression profiles of 18 AAA samples were selected for weighted gene co-expression network (WGCNA) analysis. The GSE12591 dataset collected mouse aortas exposed to saline (n = 6) or angiotensin II (n = 12)⁵⁸. The GSE7084

included control aortic samples from organ donors ($n = 10$) and full-thickness abdominal aortic wall samples from AAA patients ($n = 9$)⁵⁷. The GSE47472 contained full-thickness aortic wall specimens from AAA neck tissue ($n = 14$) and non-aneurysmal neck tissues from organ donors ($n = 8$). The GSE57691 included full-thickness abdominal aortic wall samples from AAA patients ($n = 49$) and normal full-thickness abdominal aortic wall specimens from organ donors ($n = 10$)⁶⁹. Mouse dataset (GSE12591) and human datasets (GSE7084, GSE47472, and GSE57691) were used to validate the hub genes. Each dataset above was processed by background correction including removal of batch effect using “sva” R package and quantile normalization with the “limma” R package⁷⁰ for further analysis.

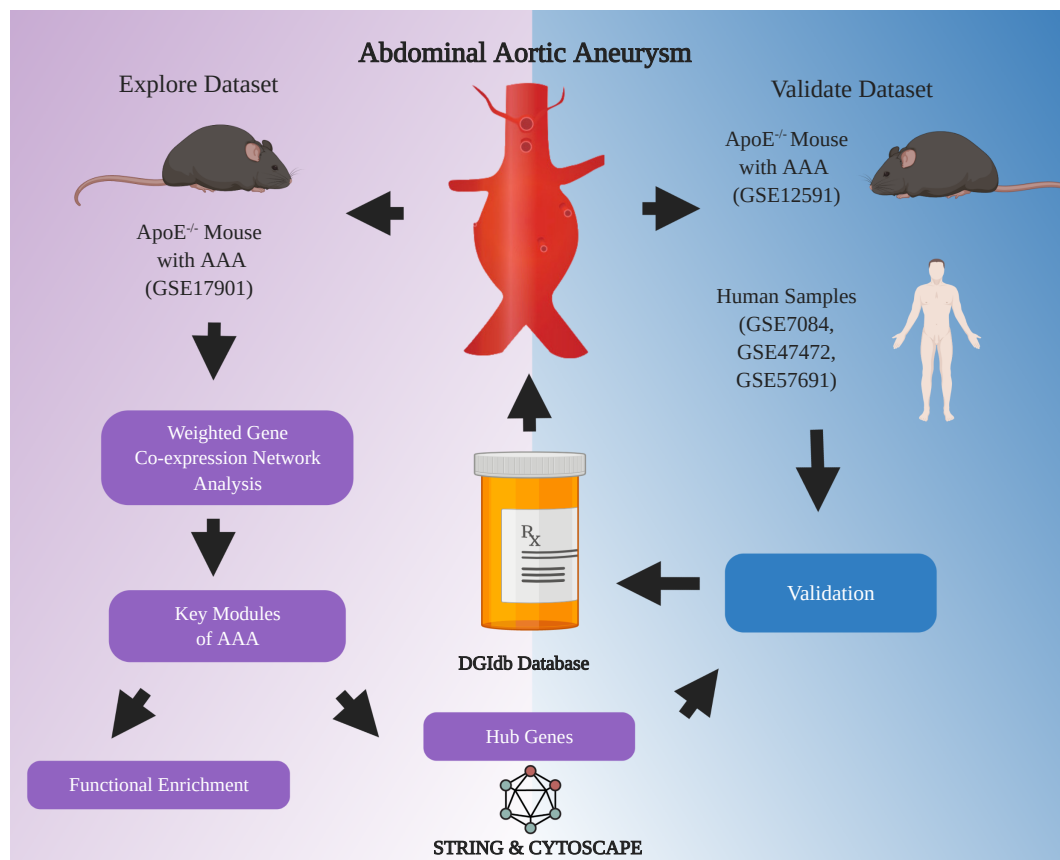


Figure 7. Flowchart of analysis in the study. GSE17901 was a mouse dataset containing AAA samples collecting on day 7, day 14 and day 28, which was used for exploring the key modules and hub genes related to AAA progression. Hub genes were identified through the STRING database and Cytoscape software. Key genes were further selected from the hub genes and validated in the mouse (GSE12591) and human (GSE7084, GSE47472 and GSE57691) AAA datasets. Finally, potential

drugs or compounds targeting these key genes were screened in the DGIdb database. AAA: abdominal aortic aneurysm.

2.2.2.2 Construction of the weighted co-expression network

We used the “WGCNA” R package to perform the weighted co-expression network analysis ⁶⁴. In the explore dataset GSE17901, the top 25% variance genes were selected for the following step analysis. The “pick Soft Threshold” function was used to determine the soft-thresholding power and construct a scale-free network. After that, gene co-expression modules were identified using the one-step network construction method and labeled with different colors. The reassign threshold was set at 0.25, and the minimum number of genes in each module was 30.

2.2.2.3 Selection of key modules

To explore the modules significantly associated with AAA progression, we calculated the relevancy between module eigengene (ME), which summarizes each module’s gene expression profiles. The correlation results were shown using the “ggcorrplot” R package ⁷¹. Furthermore, Gene Significance (GS) was quantified by the absolute value of the association between the gene expression and sample traits. In every module, measurement of module membership (MM) was defined as the correlation of the ME and gene expression profile. Modules with significance ($p\text{-value} < 0.05$) and relationship ($\text{correlation} > 0.6$ or < -0.6) were defined as key modules of AAA progression and used for hub gene selection.

2.2.2.4 Functional enrichment analysis of the key modules

To understand the biological meanings of genes in AAA-related key modules, we conducted Gene Ontology (GO) function enrichment analysis and Kyoto Encyclopedia of Genes and Genomes (KEGG) pathway analysis with the “clusterProfiler” R package ⁷². The top 10 results of each analysis were shown for visualization, results of adjusted $p\text{-value} < 0.05$ were considered a statistically significant difference in enrichment analysis.

2.2.2.5 Identification of hub genes in key modules

Hub genes are those that have a high degree of intramodular connectivity ⁶⁴. In this study, hub genes were defined as the top 10% of genes in key modules with the

highest connectivity. Then, we uploaded these genes into the search tool for the retrieval of the interacting genes (STRING) website (www.string-db.org) for protein-protein interaction analysis with setting the confidence > 0.4 ⁷³. Cytoscape software was used for network visualization and hub gene selection ⁷⁴. The top 10 hub genes in each module were selected with the maximal clique centrality (MCC) method using cytoHubba plugin software in Cytoscape ⁷⁵.

2.2.2.6 Hub genes validation and key genes selection

The validation of hub genes was performed by comparing the normalized gene expression value between control and AAA groups. The validate datasets GSE12591, GSE7084, GSE47472, and GSE57691 were downloaded and preprocessed as mentioned before. In the GSE12591 mouse dataset, the gene expression of the selected hub genes in AAA and controls were compared, and genes with $P < 0.05$ were confirmed as the key genes. In the GSE7084, GSE47472, and GSE57691 human datasets, genes were extracted as described for dataset GSE12591. Genes with $p < 0.05$ were confirmed as the key genes. Common genes in both the mouse dataset and human datasets were defined as the final key genes of AAA progression.

2.2.2.7 Predication of drug-gene interaction

The Drug–Gene Interaction Database (DGIdb) (<http://www.dgidb.org/>) is an online database of drug-gene interaction data aggregated from various sources, including several drug databases (DrugBank, PharmGKB, ChEMBL), clinical trial databases, and literature from PubMed ⁷⁶. The selected key genes that were considered the potential pharmaceutical targets for AAA treatment, were imported into DGIdb to explore existing drugs or small organic compounds. Results were displayed using the R packages “ggplot2” ⁷⁷ and “ggalluvial” ⁷⁸.

2.2.3 Statistical analysis

Statistical analyses were performed using Graphpad Prism. Variables were summarized as mean \pm standard deviation (SD). The unpaired Student's t-test was used to determine statistical significances between two groups. The number of technical and experimental replicates can be found in the figure legends for each experiment. P values less than 0.05 were considered significant and represented graphically as *, $P < 0.05$; **, $P < 0.01$; ***, $P < 0.001$, unless otherwise indicated.

3 RESULTS

3.1 Influence of blue light irradiation on endothelial cells

3.1.1 Effect of blue light on cell viability

To gain a preliminary understanding of the blue light irradiation on endothelial cells, we exposed HUVECs to different irradiation times, which was modified according to previous studies (Parameters are shown in the Table in method part) ^{79–81}. Using the XTT assay with a broad range of irradiation times, we found HUVECs responded biphasically to the blue light exposure. Short irradiation times increased the cell viability, while treatment over a longer duration decreased the cell viability (**Figure 8**). The highest cell viability was obtained with 12 min irradiation. Here cells showed a 20.2% increase with irradiance 10 mW/cm² as compared to control. An 18% rise was observed with irradiance 20 mW/cm² as compared to the control. The cell viability dropped to 71% (10 mW/cm² group) and 62% (20 mW/cm² group) compared to control after 2 hours irradiation (**Figure 8**).

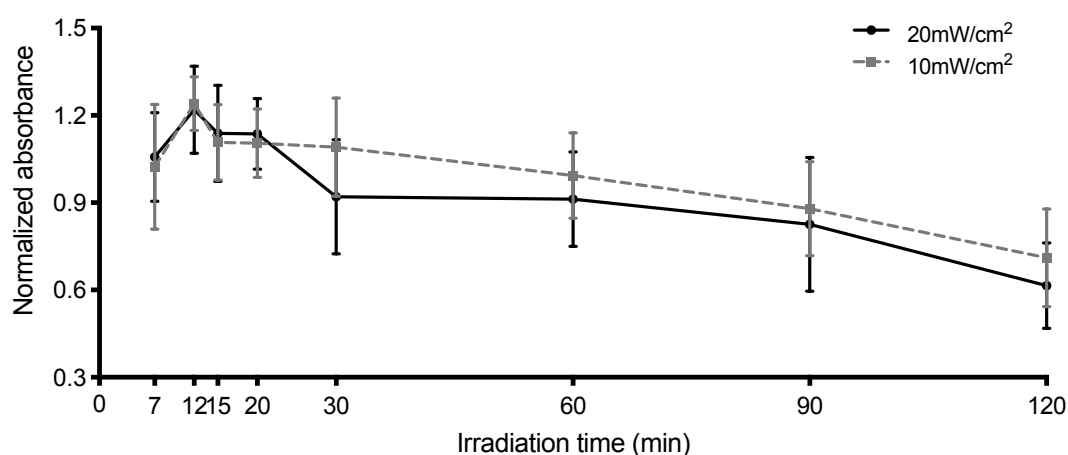


Figure 8. Changes in the cell viability of HUVECs following different blue light fluences. XTT assay at 24 hours after irradiation. Normalized

absorbance was calculated versus non-irradiated controls. Data are shown as mean \pm SD (n = 3 repetitions).

Furthermore, we narrowed the intervals of the irradiation times. The biphasic curve showed that the time point with the highest cell viability was 12 mins (13% increase in 10 mW/cm² group, 9% increase in 20 mW/cm² group). The cell viability also decreased with the prolongation of blue light irradiation (**Figure 9**).

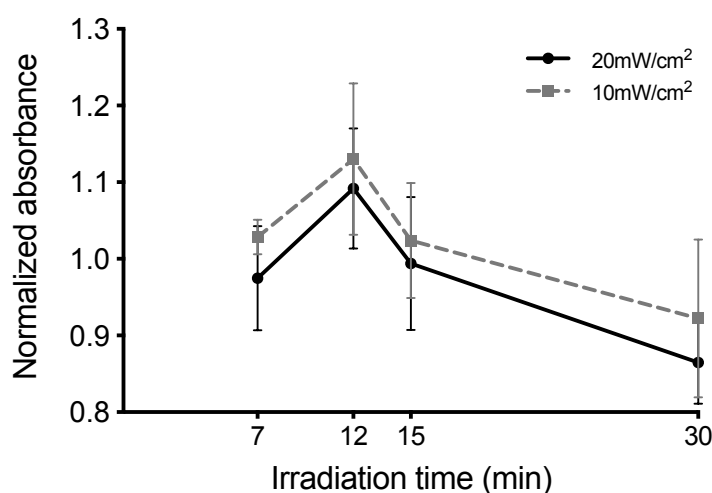


Figure 9. Cell viability changes of HUVECs after different durations of blue light irradiation. XTT assay was performed 24 hours after irradiation. Normalized absorbance was calculated versus non-irradiated controls. Data are shown as mean \pm SD (n = 3 repetitions).

The biphasic effect of blue light on HUVECs was further confirmed with BrdU assays. The result showed a similar trend: the cell proliferation was promoted after short times of irradiation, especially after 12 mins irradiation (7.6% and 7.4% compared to control, with 10 mW/cm² and 20 mW/cm², respectively). At 30 minutes it decreased to 91% and 86% as compared to controls, with 10 mW/cm² and 20 mW/cm² respectively (**Figure 10**). Again, the time point of 12

mins with 10 mW/cm² and 20 mW/cm² showed the most apparent promotion effect on cell viability and proliferation.

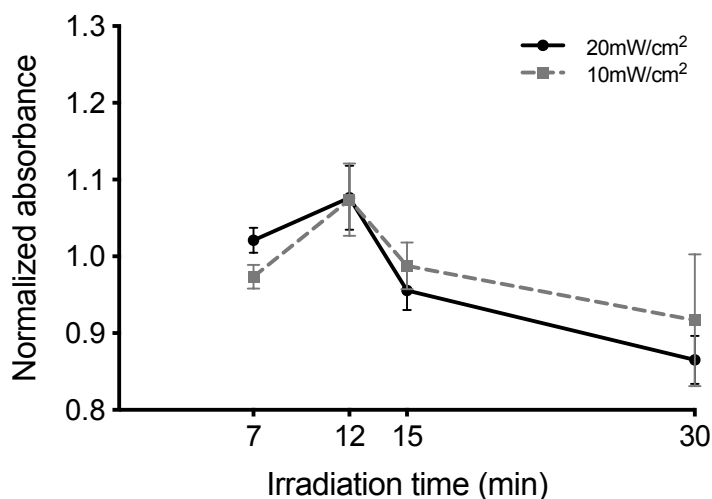


Figure 10. Changes in the cell proliferation of HUVECs following different blue light fluences. BrdU assays were performed 24 hours after irradiation. Normalized absorbance was calculated versus non-irradiated controls. Data are shown as mean \pm SD (n = 3 repetitions).

To further explore the effect of irradiance on HUVECs, we performed the XTT assay with different irradiances for 12 minutes. **Figure 11** showed that: 1. With the increase of irradiances, a biphasic response was observed in the cell viability assays; 2. Low irradiance of blue light illumination promoted cell viability. Here 10 mW/cm² over 12 mins showed the most increase (7.2%). The cell viability decreased to 84.7% when cells were irradiated with 40 mW/cm². Based on these results, two parameters were chosen for the following experiments: a low fluence group (10 mW/cm² * 12 min, 7.2 J/cm²) and a high fluence group (40 mW/cm² * 12 min, 28.8 J/cm²).

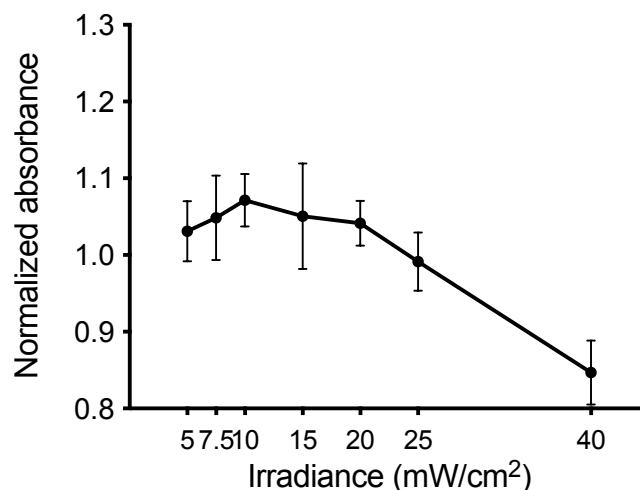


Figure 11. Changes in the cell viability of HUVECs following irradiance over the fixed time point of 12 minutes of XTT assay at 24 hours after irradiation. Normalized absorbance was calculated versus non-irradiated controls. Data are shown as mean \pm SD (n = 3 repetitions).

3.1.2 Effect of blue light on redox metabolism and apoptosis in cells

Previous studies suggested that blue light irradiation could increase the intercellular ROS level^{82,83}, so we evaluated ROS changes after blue light irradiation HUVECs using the Grx1-roGFP3 redox sensor and DCFH-DA dye. Grx1-roGFP3 is a redox sensor that can be used to detect the oxidation and reduction reaction in cells dynamically. In this study, the ROS level detected by the sensor was immediately increased after irradiation (time point: 0.4 h) (**Figure 12**), especially in the high fluence treatment group (40 mW/cm² * 12 min) with a 12% increase. In contrast, the low fluence irradiation (10 mW/cm² * 12 min) only led to a 4.9% ROS increase. This upregulation of ROS recovered to baseline after 24 hours (**Figure 12**).

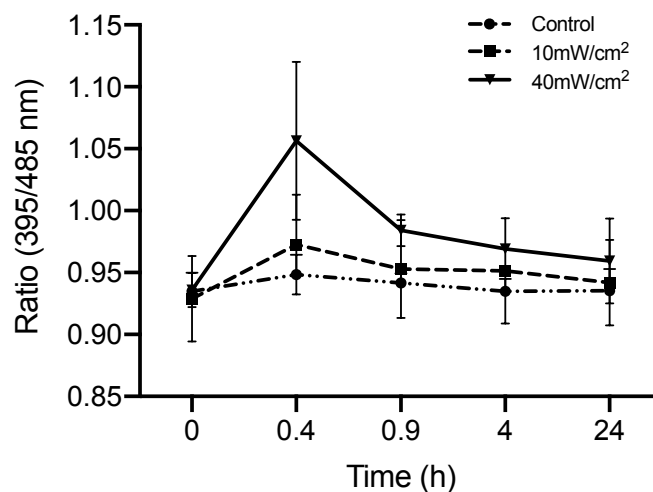


Figure 12. Dynamic ROS changes of HUVECs as determined with the redox sensor following blue light exposure to either low fluence (10 mW/cm² * 12 min) or high fluence (40 mW/cm² * 12 min). Data are shown as mean \pm SD (n = 3 repetitions).

And the same ROS changes were observed in the DCFH-DA dye staining assay. High fluence irradiation (40 mW/cm² * 12 min) increased ROS by 23% ($p < 0.01$) as compared to the low fluence after irradiation. ROS levels returned to pre-irradiation level 24 hours post-irradiation (**Figure 13**). So here, we found that blue light could increase the ROS production of HUVECs in a fluence-dependent manner, and the increase of ROS would return to normal after retreating the blue light irradiation.

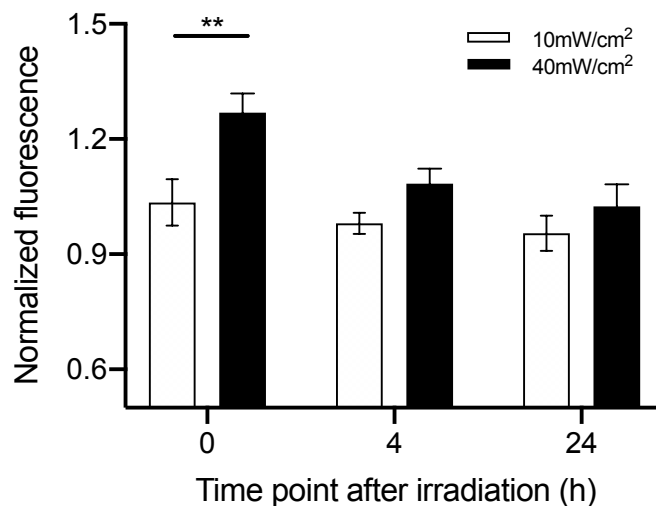


Figure 13. Changes in the ROS levels in HUVECs following exposure to either low fluence (10 mW/cm² * 12 min) or high fluence (40 mW/cm² * 12 min) using the DCFH-DA assay after irradiation. Normalized fluorescence was calculated versus non-irradiated controls. Data are shown as mean \pm SD (n = 3 repetitions. **p<0.01).

Since ROS overproduction can cause cell death⁸⁴, we further evaluated if blue light irradiation mediated ROS increase led to apoptosis with the above irradiation parameters. Here, we performed the Annexin V and PI staining on the HUVEC cells after irradiation. Annexin V staining could show the early stage of apoptosis cells and PI indicates the late apoptotic state. The percentage of apoptosis cells after irradiation was evaluated using a flow cytometer. From the results (**Figure 14A and 14B**), no evident apoptosis was observed after low fluence illumination and in the control group, while the high fluence slightly increased the number of apoptotic cells by 3.6% as compared to the control group (p<0.05).

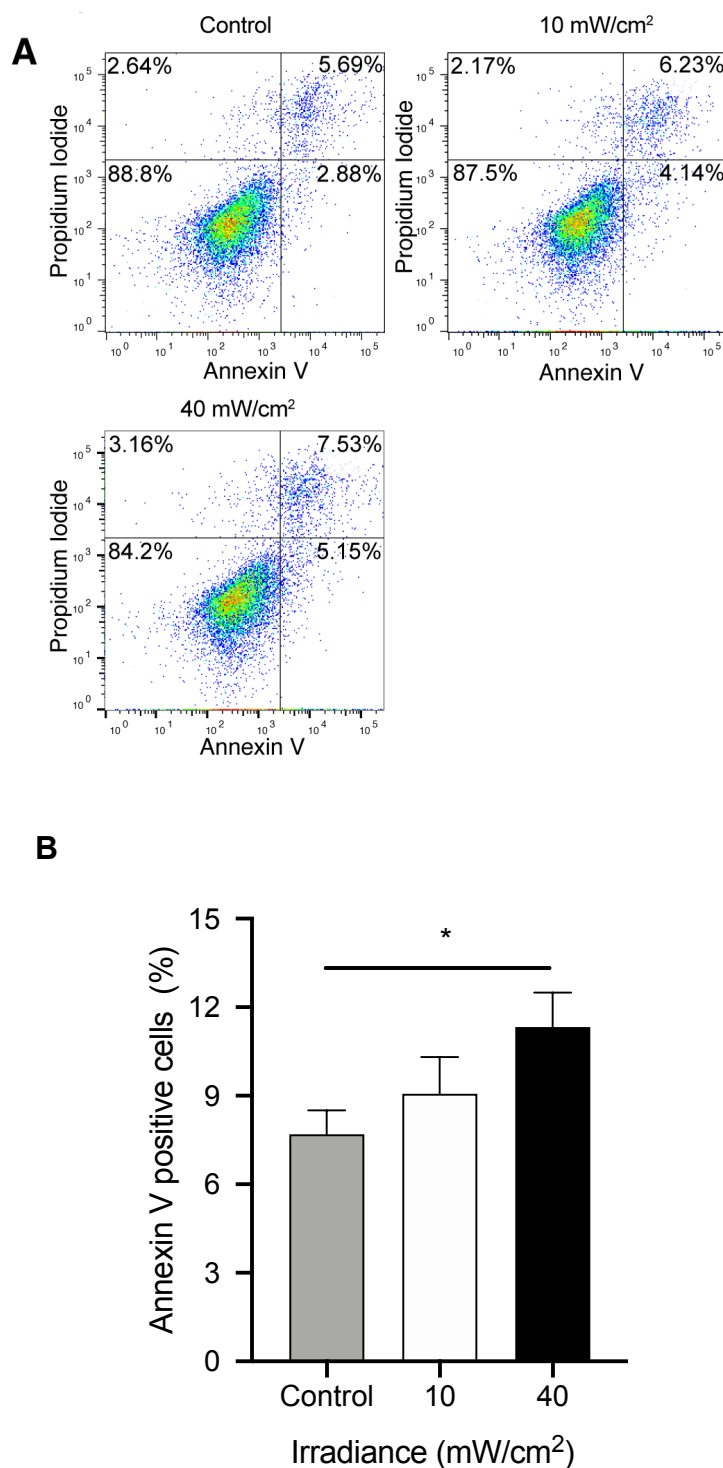
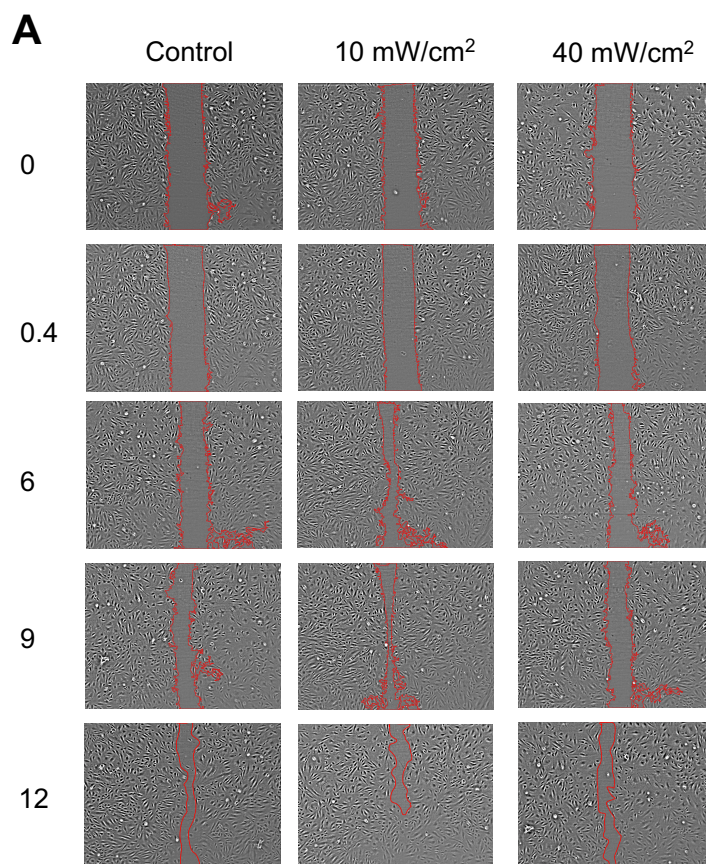


Figure 14. Apoptosis changes in HUVECs following exposure to either low fluence (10 mW/cm² * 12 min) or high fluence (40 mW/cm² * 12 min) after irradiation using flow cytometer. (A) Representative results of Annexin V PI staining of HUVEC cells following exposure to either low fluence (10 mW/cm² * 12 min) or high fluence (40 mW/cm² * 12 min) measured by flow cytometry at 24 hours after irradiation. (B) Quantification of cell apoptosis

induced by blue light. Annexin V+/PI- and Annexin V+/PI+ populations were considered as apoptotic cells. Data are shown as mean \pm SD (n = 3 repetitions. *p<0.05).

3.1.3 Effect of blue light on cell migration

To explore whether blue light could also influence cell migration, the scratch assay was performed. From the images acquired at different time points after blue light irradiation, HUVECs irradiated by a low fluence (10 mW/cm² * 12 min) closed the wound significantly faster than the control cells after 9 h (p<0.05, compared with the control group), and no significant difference were observed in cells irradiated by high fluence (40 mW/cm² * 12 min) (**Figure 15A and 15B**).



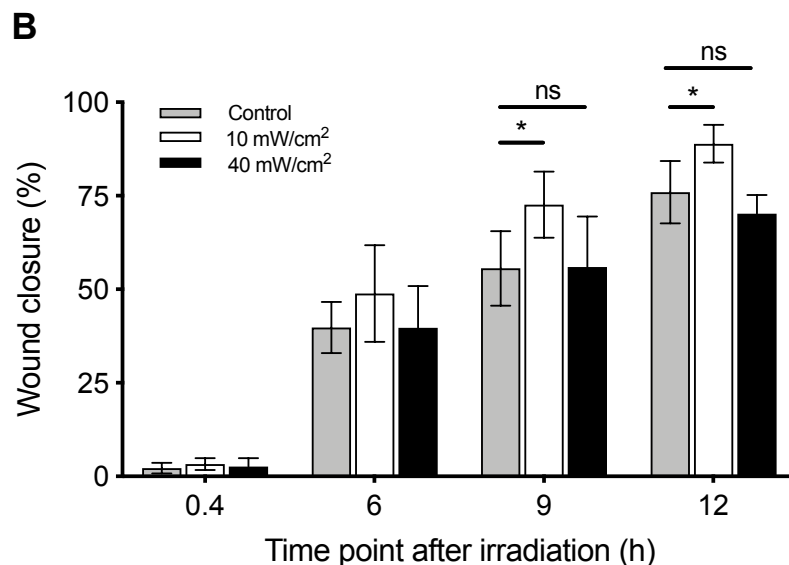


Figure 15. Cell migration determined by the scratch assay following exposure to either low fluence (10 mW/cm² * 12 min) or high fluence (40 mW/cm² * 12 min) after blue light irradiation. (A) Representative images of the scratch assay were taken at 0, 0.4, 6, 9 and 12 hours after irradiation. (B) Quantification of data from the scratch assay. Data are shown as mean \pm SD (n = 3 repetitions. *p<0.05; ns: not significant).

To further confirm the blue light effect on cell migration, the trans-well assay was performed. The results of 6 hours after light treatment showed low fluence irradiation prompted the migration through the membranes, about 38% increase as compared to control cells ($p < 0.01$) (**Figure 16A and 16B**). Contrary to the findings of the scratch assay, blue light irradiation with a high fluence inhibited the migration of cells ($p < 0.05$) (**Figure 16A and 16B**). Taken together with the two migration assays, we can conclude that blue light irradiation also induced a biphasic effect on cell migration.

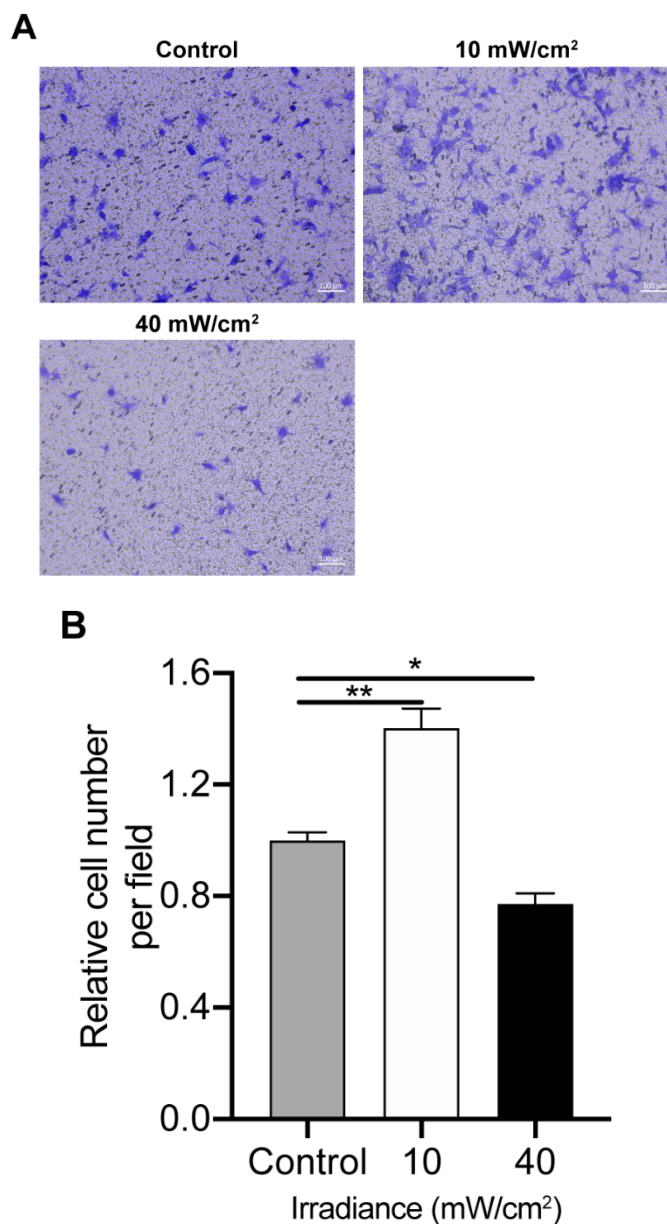


Figure 16. Cell migration determined by the trans-well assay following exposure to either low fluence (10 mW/cm² * 12 min) or high fluence (40 mW/cm² * 12 min) after blue light irradiation. (A) Representative images of the trans-well assay at 6 hours after irradiation. (B) Quantification of data from the trans-well assays. Data are shown as mean \pm SD (n = 3 repetitions. *p<0.05, **p<0.01)

3.1.4 Effect of blue light on cell angiogenesis

To analyze the effect of blue light irradiation on the angiogenic function of HUVECs, we performed tube formation and spheroid sprouting assays. Figure 10 showed that 6 hours after blue light treatment, longer tube-lengths formed in the low fluence group ($p < 0.01$ in comparison to the non-irradiated group), and fewer tubes formed in the high fluence group ($p < 0.05$) (**Figure 17A and 17B**). Likewise, in the sprouting assay, more sprouting was observed in the low fluence treated group while sprouting of HUVEC cells spheroids was inhibited by blue light irradiation at higher fluence (**Figure 17C**). Here, we could conclude that blue light affected the cell angiogenic function biophasically in vitro.

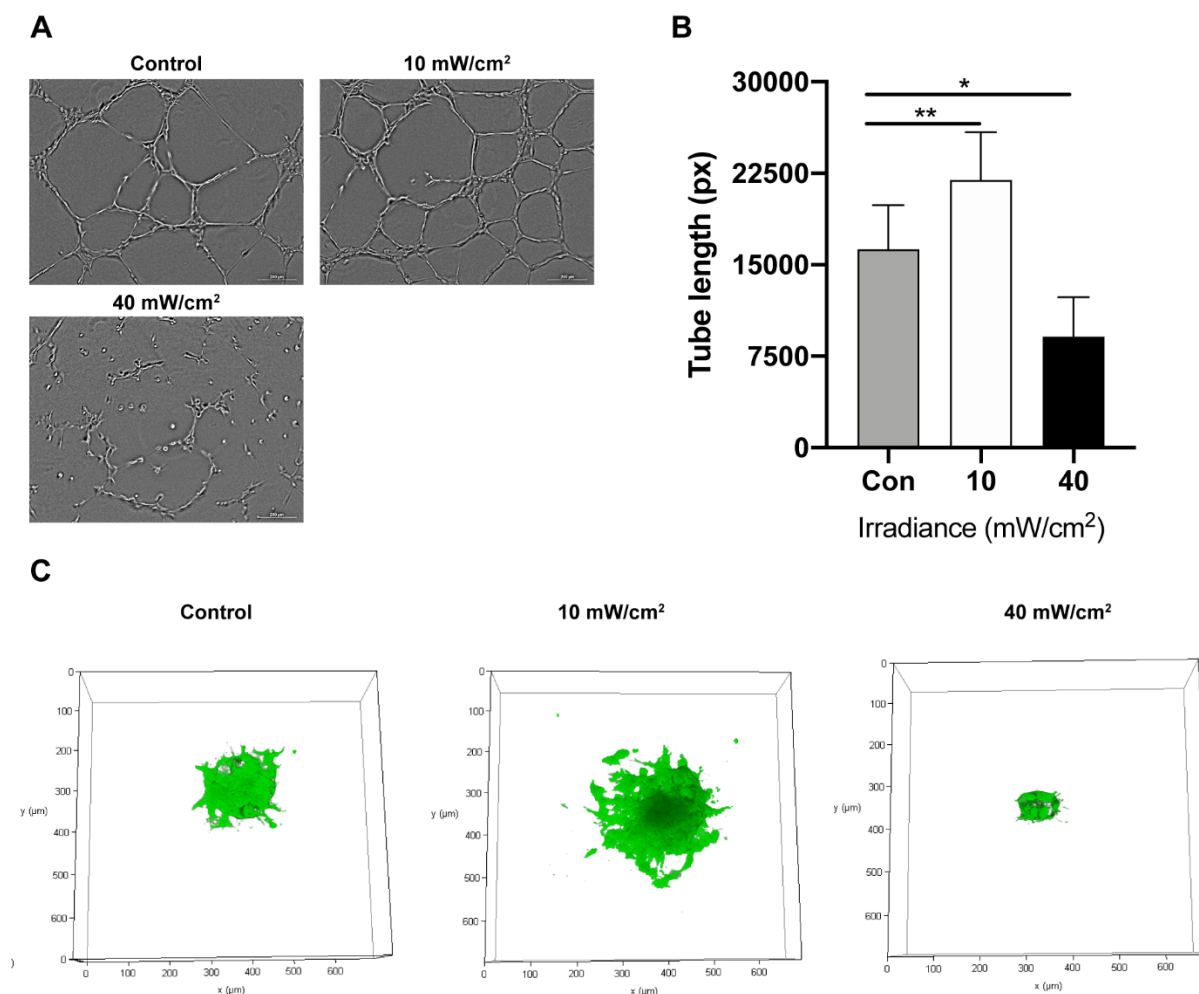


Figure 17. Blue light affects tube formation and sprouting in HUVECs. (A)

Representative images of the tube formation assay of HUVEC cells following

exposure to either low fluence (10 mW/cm² * 12 min) or high fluence (40 mW/cm² * 12 min) illumination at 6 hours after irradiation. (B) Quantification of data from tube formation assays. Data are shown as mean ± SD (n = 3 repetitions. *p<0.05, **p<0.01). (C) Representative images of the spheroid sprouting assay of HUVEC cells with GFP following exposure to either low fluence (10 mW/cm² * 12 min) or high fluence (40 mW/cm² * 12 min) at 6 hours after irradiation.

3.1.5 Gene expression analysis of cells with different fluences of blue light irradiation

Following different fluences of irradiation, gene expression profiling was performed by RNA sequencing, with three replicates for each condition: non-irradiated control, low fluence and high fluence treatment. Cells were harvested and RNA extracted 24 hours after the blue light irradiation. All RNA samples passed the RNA quality control (RIN >9.8).

The principal components analysis (PCA) showed three distinct clusters corresponding to non-irradiated control, low fluence and high fluence treatment, which indicated the differences of the gene expression among the three clusters (**Figure 18**).

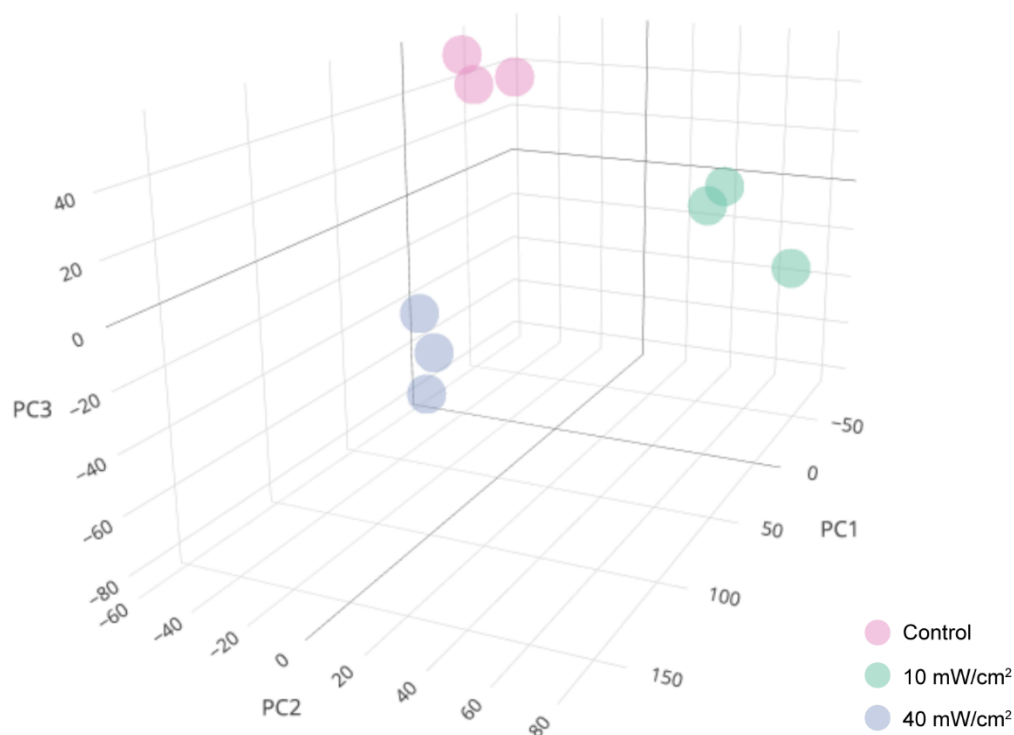


Figure 18. Principal component analysis (PCA) of RNA-seq data from HUVECs in non-irradiated control, low fluence (10 mW/cm² * 12 min) and high fluence (40 mW/cm² * 12 min) treatment group.

From the gene expression profiling with RNA-seq, 2263 significant genes (p-value < 0.05) were differentially expressed in the low fluence group compared to control group of which 1079 genes are downregulated (logFC < 0) and 1184 genes were upregulated (logFC > 0). In the high fluence vs control group, 1668 significantly expressed genes were screened out (p-value < 0.05), consisting of 749 down-regulated genes (logFC < 0) and 919 up-regulated genes (logFC > 0) (**Table 4**).

Table 4. The number of significantly differentially expressed (either up- and down-regulated genes) in HUVECs following blue light treatment with low fluence (10 mW/cm² * 12 min) and high fluence (40 mW/cm² * 12 min) compared with non-irradiated control.

Treatment group	Significantly differentially expressed genes		
	Down-regulated genes	Up-regulated genes	Total
10 mW/cm ²	1079	1184	2263
40 mW/cm ²	749	919	1668

After that, Gene Set Enrichment Analysis (GSEA) was performed using the Kyoto Encyclopedia of Genes and Genomes (KEGG) database. The Normalized Enrichment Scores (NES) were used to reveal the pathway or gene set distributions, and negative or positive NES indicated respectively down- or up-regulated pathways or gene sets. **Table 5** lists the numbers of de-regulated KEGG pathways in HUVECs with different irradiance of blue light treatment.

Table 5. The number of differentially expressed KEGG pathways in HUVECs treated with low fluence (10 mW/cm² * 12 min) and high fluence (40 mW/cm² * 12 min) compared with non-irradiated controls.

Treatment group	10 mW/cm ²	40 mW/cm ²
De-regulated KEGG pathways	92	75
Up-regulated pathways	82	66
Down-regulated pathways	10	9

In the low fluence group, a total of 92 KEGG pathways were de-regulated (p-value<0.05), 89% of the pathways are up-regulated (NES >0), and only 10 pathways are down-regulated (NES<0). There are 75 de-regulated pathways in the high fluence group, of which 66 pathways (88%) are up-regulated (NES >0) and 9 pathways are down-regulated (NES<0).

The most affected KEGG pathways (NES >1.5 or NES <-1.5) have been considered for the subsequent analysis. **Table 6** lists these differentially pathways and their main category (level 1 KEGG category) of biological function. As described above, most affected KEGG pathways are up-regulated both in the low fluence group and high fluence group (88.3%, 86.4%, respectively).

Table 6. Number of the most affected KEGG pathways in HUVECs treated with low fluence (10 mW/cm² * 12 min) and high fluence (40 mW/cm² * 12 min) compared with non-irradiated control.

Treatment group	10 mW/cm ²	40 mW/cm ²
Most affected KEGG pathways	60	59
Up-regulated pathways	53	51
Down-regulated pathways	7	8
Level 1 KEGG category	60	59
Cellular Processes	3	6
Environmental Information Processing	11	3
Genetic Information Processing	1	7
Human Diseases	15	8
Metabolism	4	33
Organismal Systems	26	2

In the low fluence group, the biggest part of the level 1 KEGG functional category was the “Organismal systems” (43.3%), followed by the “Human Diseases” (25%) (**Table 6**). Furthermore, the “Signal transduction” pathway occupies the highest proportion (18%) (**Figure 19**) in the level 2 KEGG functional category, in which the “Hippo_singaling pathway” was down-regulated and the other 10 pathways are up-regulated. “Metabolism” pathways have the highest percentage of level 1 KEGG functional categories in the high fluence group (55.9%), especially the “Carbohydrate metabolism”

(25.3% in the level 2 KEGG functional category) in which all the pathways are up-regulated (**Figure 20**).

Based on the above results, we focused on the VEGF pathway (NSE = 1.61) in the low fluence group. In the high fluence group, the enriched p53 pathway (NES =2.04) was chosen, as they were reported to play essential roles in angiogenesis (**Figure 21A and 21B**).

RESULTS

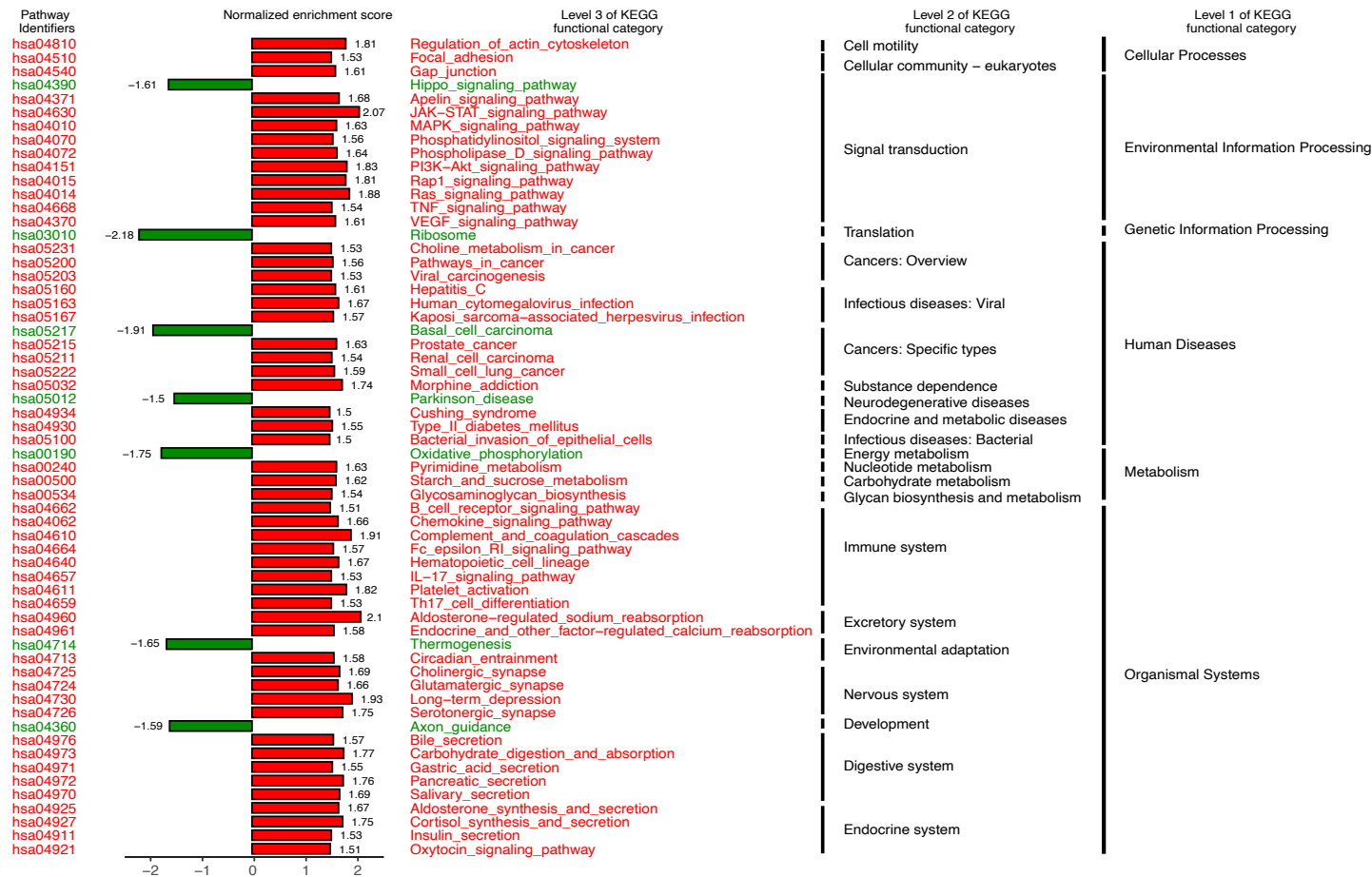


Figure 19. KEGG pathway enrichment analysis of low fluence ($10 \text{ mW/cm}^2 \cdot 12 \text{ min}$) versus the non-irradiated control group. Significantly different functional KEGG categories ($\text{NES} > 1.5$ or < -1.5 and $p < 0.05$) are shown.

RESULTS

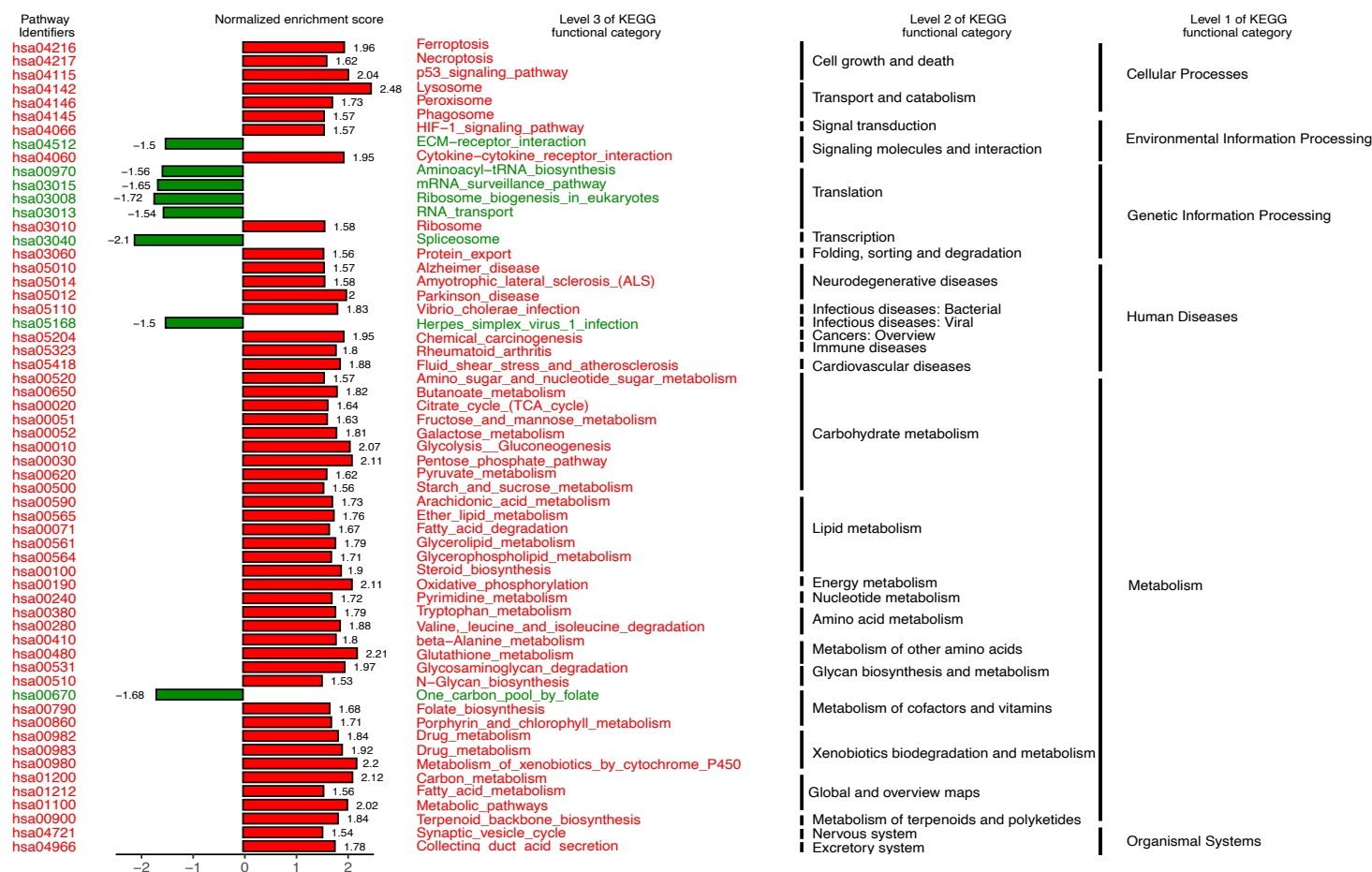


Figure 20. KEGG pathway enrichment analysis of high fluence (40 mW/cm² * 12 min) versus the non-irradiated control group. Significantly different functional KEGG categories (NES >1.5 or <-1.5 and p < 0.05) are shown.

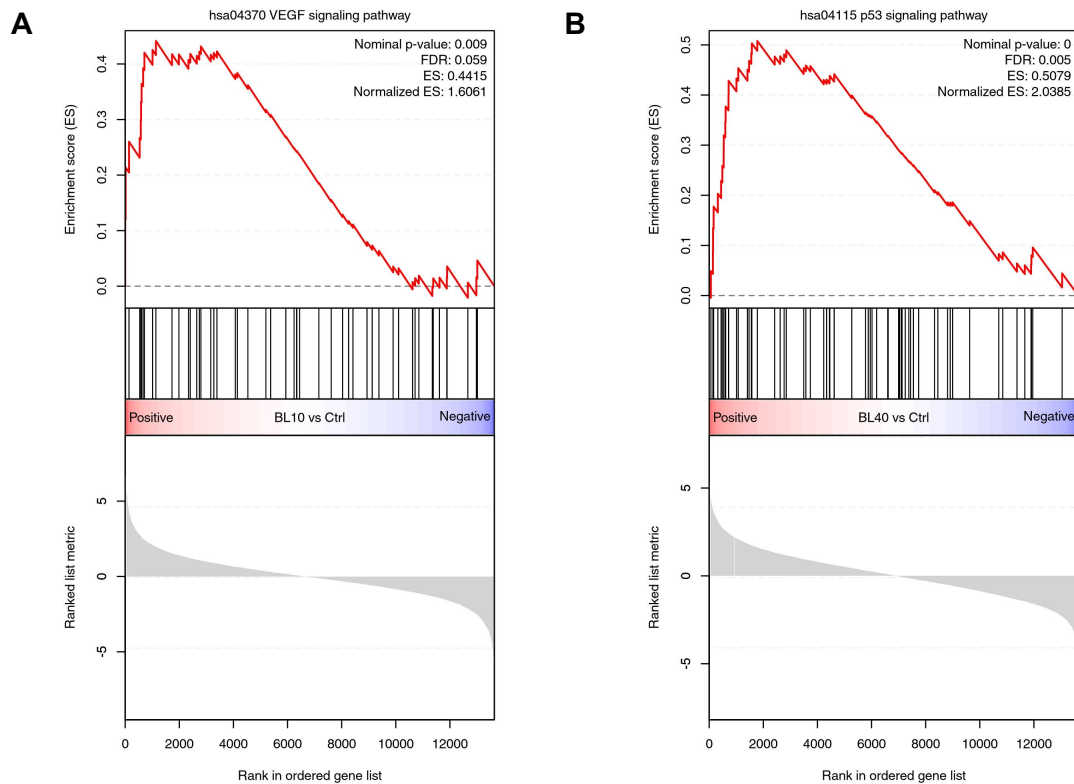


Figure 21. Gene set enrichment analysis of the interested pathways. (A) VEGF signaling pathway was up-regulated in the low fluence ($10 \text{ mW/cm}^2 * 12 \text{ min}$) group. (B) p53 signaling pathway was up-regulated in the high fluence ($40 \text{ mW/cm}^2 * 12 \text{ min}$) group.

3.1.6 Verification of genes in interested pathways with qPCR

We selected the genes which are essential in each pathway as reported. The validation was performed with RNA samples derived 24 h after blue light irradiation. QPCR results partially matched the RNA sequencing results. We found in the VEGF pathway two genes enriched in the low fluence group, PLA2G4A and PTGS2 were highly expressed after low fluence blue light irradiation. In the enriched p53 pathway of the high fluence group, CASP9 and BAX were significantly up-regulated (**Figure 22A and 22B**).

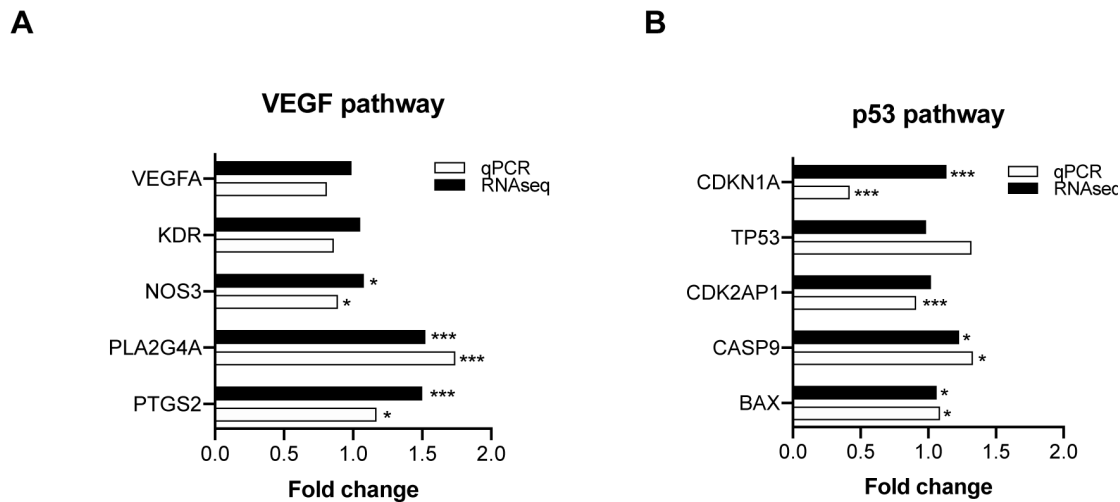


Figure 22. qPCR validation of genes in the interested pathways. (A) qPCR validation of genes in the VEGF signaling pathway and comparison with RNA-seq data. Fold change was normalized with control. $n = 3$ repetitions, * $p < 0.05$, *** $p < 0.001$. (B) qPCR validation of genes in the p53 signaling pathway and comparison with RNA-seq data. Fold change was normalized with control. * $p < 0.05$, *** $p < 0.001$.

3.2 Weighted gene co-expression network analysis in the development of abdominal aortic aneurysm

The present work was published in *Biomedicines* 2021, 9(5), 546; <https://doi.org/10.3390/biomedicines9050546>.

3.2.1 Construction of weighted gene co-expression network

After the data preparation of the explore dataset GSE17901 using the “WGCNA” package, we included 17 samples to construct a weighted co-expression network. Soft power 9 was selected as the soft thresholding to construct a weighted adjacency matrix (scale-free $R^2 = 0.85$) (**Figure 23A**). 15 co-expression modules were obtained, among which the turquoise module (1394 genes) was the biggest cluster, followed by the blue module (897 genes), brown module (793 genes), and yellow module (586 genes) (**Figure 23B**).

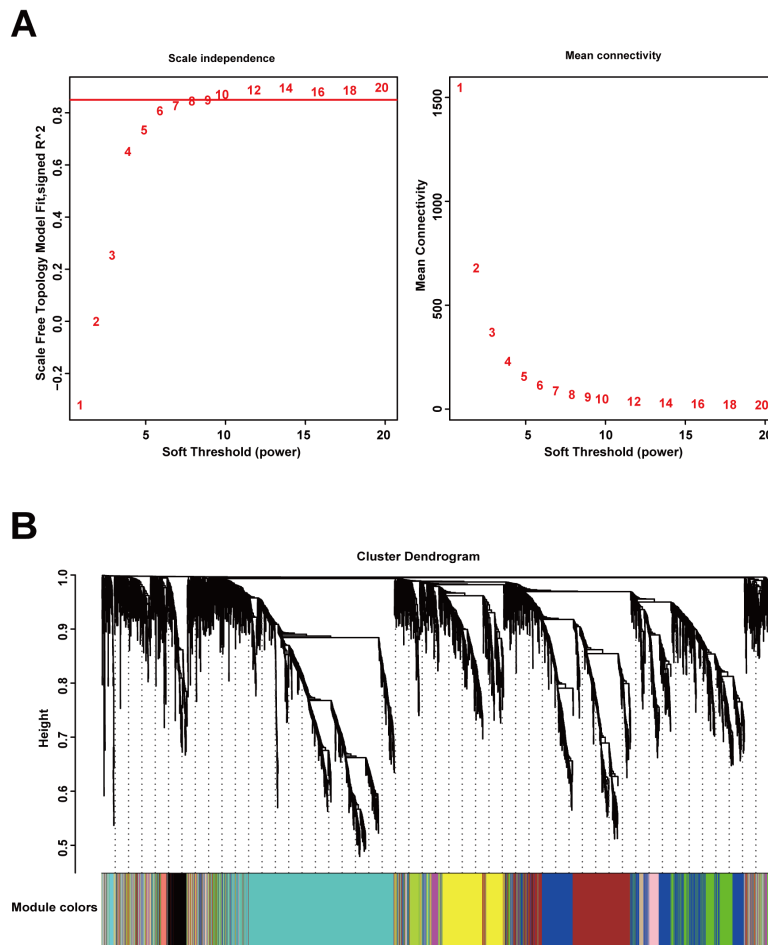


Figure 23. Construction of gene co-expression network by WGCNA. (A) Determination of soft-thresholding power for scale-free network construction. Here, we set the coefficient threshold at 0.85, and the soft-threshold was 9. (B) Cluster analysis of dendrogram and identification of co-expressed modules. In this study, we got 15 related co-expression modules.

3.2.2 Construction of module-trait relationships and detection of key modules

The mouse AAA samples consisting of the entire suprarenal aorta in the explore dataset GSE17901 were collected on day7, day14, and day28. Some aneurysmal samples were caused by local dissection of the suprarenal aorta⁵⁹. The connection between sample traits above and modules was calculated by the correlation between ME and sample traits. As is shown in **Figure 24**, blue (R^2 : -0.64, p :0.006), green (R^2 : 0.61, p :0.01), and brown (R^2 : 0.61, p :0.009) modules were strongly related to the time trait, representing the progression of AAA. Blue (R^2 : 0.77, p : 0.0003) and green modules (R^2 : -0.85, p : 0.00002) also significantly correlated with the dissection

sample trait. We defined these three modules as key modules which were highly correlated with AAA.

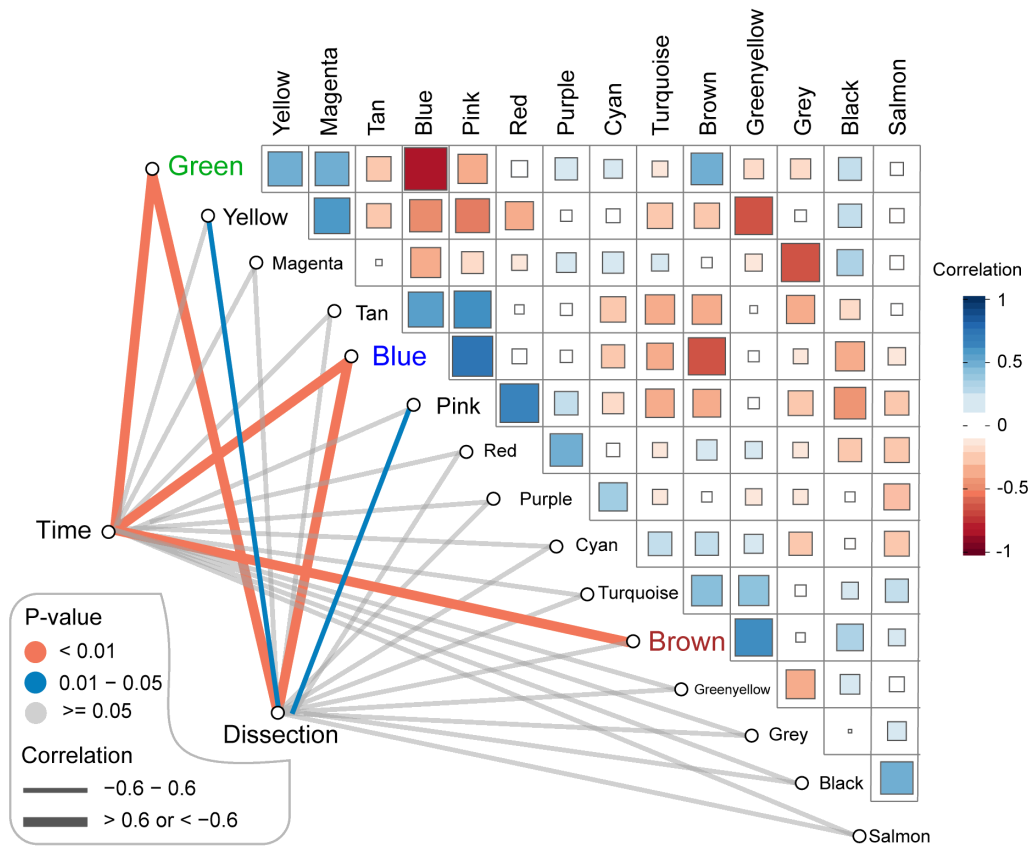


Figure 24. Identification of the key modules associated with AAA progression.

Green, blue and brown modules were highly correlated (Correlation > 0.6 or -0.6 and P-value < 0.01) to the time of sample collecting which stands for AAA progression. Green and blue modules were also related to the occurrence of dissection in some of the murine vessel specimens (Correlation > 0.6 or -0.6 and P-value < 0.01). AAA: abdominal aortic aneurysm.

3.2.3 Functional enrichment analysis of genes in the module

To understand the biological functions of key modules related to AAA progression, we further performed GO and KEGG enrichment analysis on genes in each key module. The top 10 results of GO enrichment analysis showed that genes in the blue module (count > 25) were mainly involved in the organelle fission, regulation of mitotic cell cycle, nuclear division, mitotic nuclear division and cell chemotaxis (**Figure 25A**). Genes in the green module (count > 10) engaged in the regulation of

GTPase activity, positive regulation of GTPase activity and Protein processing (**Figure 25B**). Brown module enriched genes involved in cellular metabolic processes, especially cofactor metabolism, purine-containing compound metabolism, and purine nucleotide metabolism, fatty acid metabolic process, coenzyme metabolic process (count > 30) (**Figure 25C**).

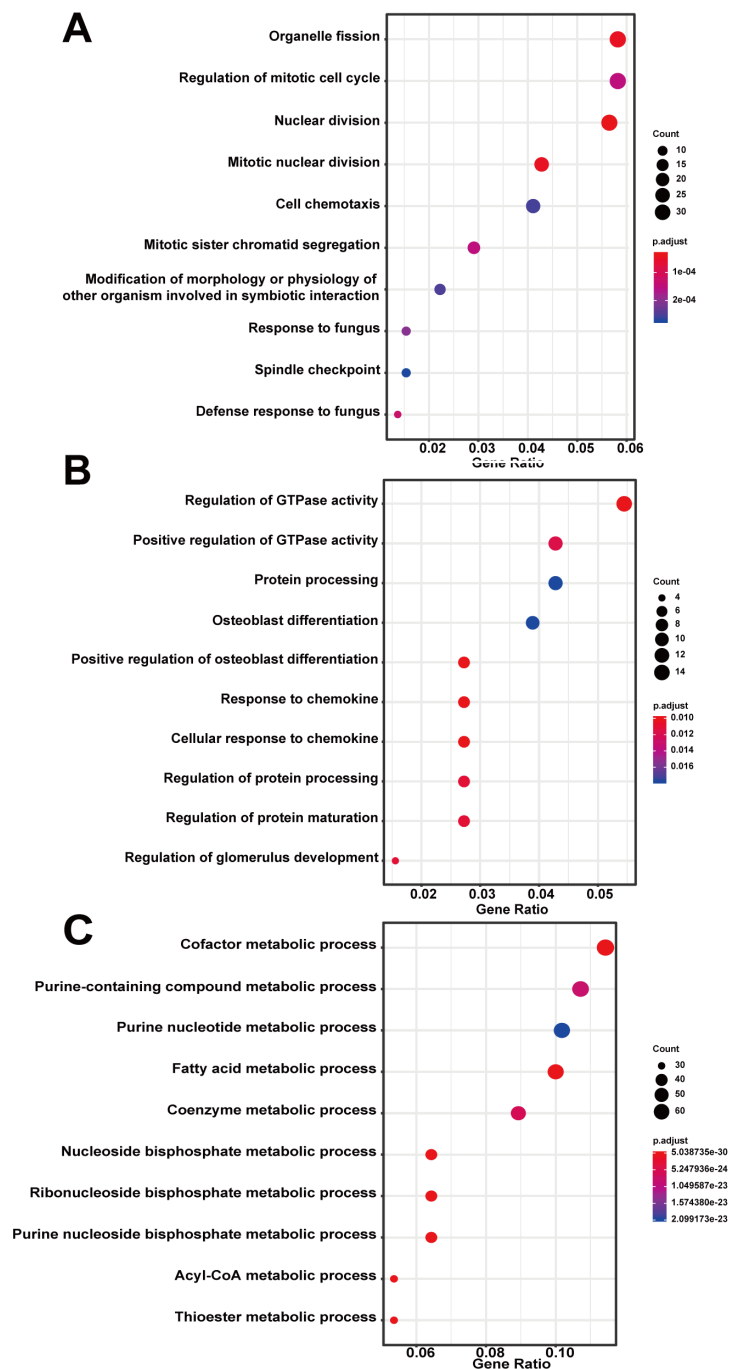


Figure 25. Gene ontology enrichment analysis of key modules of AAA progression. (A) Blue module. (B) Green module. (C) Brown module. Count: the

number of genes in the given GO term. Gene ratio: the percentage of total genes in the given GO term.

From the KEGG enrichment analysis, the fluid shear stress and atherosclerosis pathway were enriched in the blue module (rich factor = 0.09), which is highly related to the progression of AAAs (**Figure 26A**). Genes in the green module were clustered in the regulation of lipolysis in the adipocyte pathway (rich factor = 0.13) (**Figure 26B**). The most enriched pathway in the brown module was the citrate cycle (TCA cycle) pathway, of which the rich factor was 0.54 (**Figure 26C**).

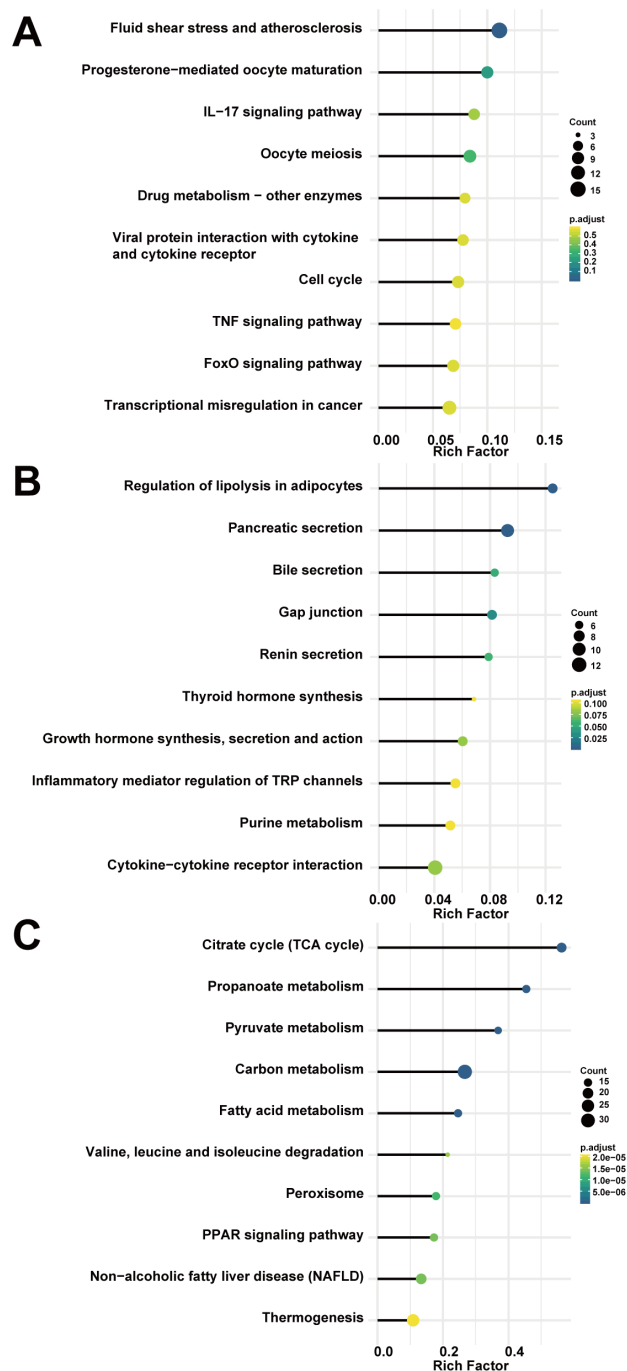


Figure 26. KEGG pathway enrichment analysis of key modules of AAA progression. (A) Blue module. (B) Green module. (C) Brown module. Count: the number of genes in the given KEGG pathway. Rich factor: the ratio of the number of genes annotated in a pathway to the number of all genes annotated in this pathway.

3.2.4 Identification of hub genes in the key modules

To explore the hub genes which may regulate the AAA development, the top 10% genes with high connectivity in each module were imported into the String online database for protein-protein interaction (PPI) detection. The PPI networks were formed in the Cytoscape software. With the cytoHubba plugin using the MCC method, the top 10 hub genes were identified from the key modules, namely, in the blue module (Ccr5, Fpr2, Ccr2, Fpr1, P2ry12, Hcar1, Ppbp, Aif1, Sirpb1b, Clec4n), green module (Gnai1, Adcy5, Adcy3, Rnase2a, Cxcl13, Clca1, Ear10, Ear1, Npr1, Ccl11), and brown module (Lpl, Dgat2, Fasn, Acacb, Lpin1, Acsl1, Mogat1, Lep, Ucp3, Pdk4) (Table 7).

Table 7. Top 10 ranked genes in key modules with the MCC method in cytoHubba.

Catalog	Key Modules		
	Blue	Green	Brown
Top 10 Gene	Ccr5	Gnai1	Lpl
	Fpr2	Adcy5	Dgat2
	Ccr2	Adcy3	Fasn
	Fpr1	Rnase2a	Acacb
	P2ry12	Cxcl13	Lpin1
	Hcar1	Clca1	Acsl1
	Ppbp	Ear10	Mogat1
	Aif1	Ear1	Lep
	Sirpb1b	Npr1	Ucp3
	Clec4n	Ccl11	Pdk4

3.2.5 Hub genes validation and key genes selection

To further evaluate the hub genes identified above, we compared the gene expression from the mouse dataset GSE12591, which used the same mouse angiotensin II-induced AAA model as the explore dataset GSE17901. *Ccr5* and *P2ry12* in the blue module were significantly upregulated and *Hcar1* was significantly down-regulated in the AAA group compared with the control group (**Figure 27A**). In the green module, *Adcy5* and *Adcy3* were the significantly expressed genes in the AAA group (**Figure 27B**). All significantly expressed genes (*Dgat2*, *Fasn*, *Acacb*, *Lpin1*, *Acs11*, *Mogat1*, *Ucp3*, *Pdk4*) in the brown module were down-regulated in the AAA group (**Figure 27C**).

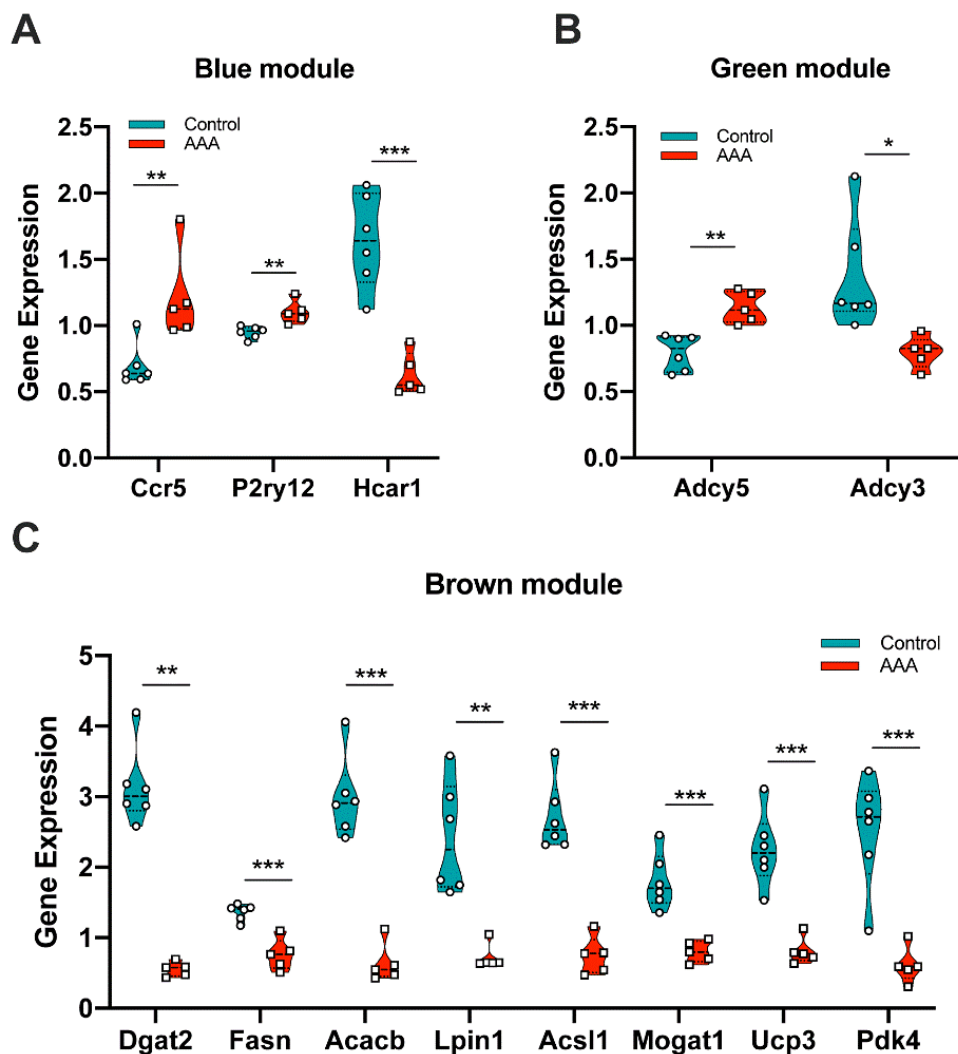


Figure 27. Validation of gene expression from hub genes in mouse dataset GSE12591. (A) *Ccr5*, *P2ry12* and *Hcar1* were differentially expressed in the blue module. (B) *Adcy5* and *Adcy3* were differentially expressed in the green module. (C) *Dgat2*, *Fasn*, *Acacb*, *Lpin1*, *Acs11*, *Mogat1*, *Ucp3* and *Pdk4* were differentially

expressed in the brown module. *: $p < 0.05$, **: $p < 0.01$, ***: $p < 0.001$ (Wilcoxon rank-sum test).

In the human AAA datasets GSE7084, GSE47472, and GSE57691, all of the significantly expressed genes were identified by comparing the full thickness abdominal aortic wall samples between healthy organ donors and AAA, shown in Table 2. Considering the individual differences within each sample, genes expressed significantly in every human dataset were defined as human key genes. CCR5, ADCY5, ADCY3, ACACB, LPIN1, ACSL1, and UCP3 were the common genes that showed up both in the mouse AAA dataset and human AAA dataset, and these were selected as the key genes in AAA progression.

Table 8. Significantly expressed hub genes in human AAA datasets.

Datasets	Key Modules		
	Blue	Green	Brown
GSE7084	CCR5, CCR2, FPR2, FPR1, AIF1	GNAI1, RNASE2, NPR1	NA
GSE47472	CCR2, PPBP	FPR2, GNAI1, RNASE2, CLCA1, LYVE1	LPIN1, UCP3
GSE57691	CCR2, PPBP, SIRPB1	FPR2, CLEC6A, ADCY5, ADCY3, CXCL13, CLCA1, CCL11	ACACB, LPIN1, ACSL1, LEP
Human	CCR5, FPR2, PPBP, AIF1, CLEC6A, SIRPB1, FPR1	CCR2, GNAI1, RNASE2, NPR1, CLCA1, LYVE1, ADCY5, ADCY3, CXCL13, CCL11	ACACB, LPIN1, ACSL1, LEP, UCP3

3.2.6 Predication of drug-gene interaction

From the above analysis, seven key genes (CCR5, ADCY5, ADCY3, ACACB, LPIN1, ACSL1, and UCP3) were selected as the potential druggable targets for AAA treatment. These genes were imported into the DGldb database for predicting drug-gene interaction. The results showed that 35 potential target drugs/compounds might be used for AAA treatment. 23 drugs targeting CCR5, among which maraviroc had the highest prediction score; seven drugs target ACACB, two drugs each target ACSL1 and ADCY5, and one drug targets LPIN1 (**Table 9, Figure 28**).

No potential drugs were identified for ADCY3 and UCP3 in the database. These 2 may also be considered potential targets in AAA treatment.

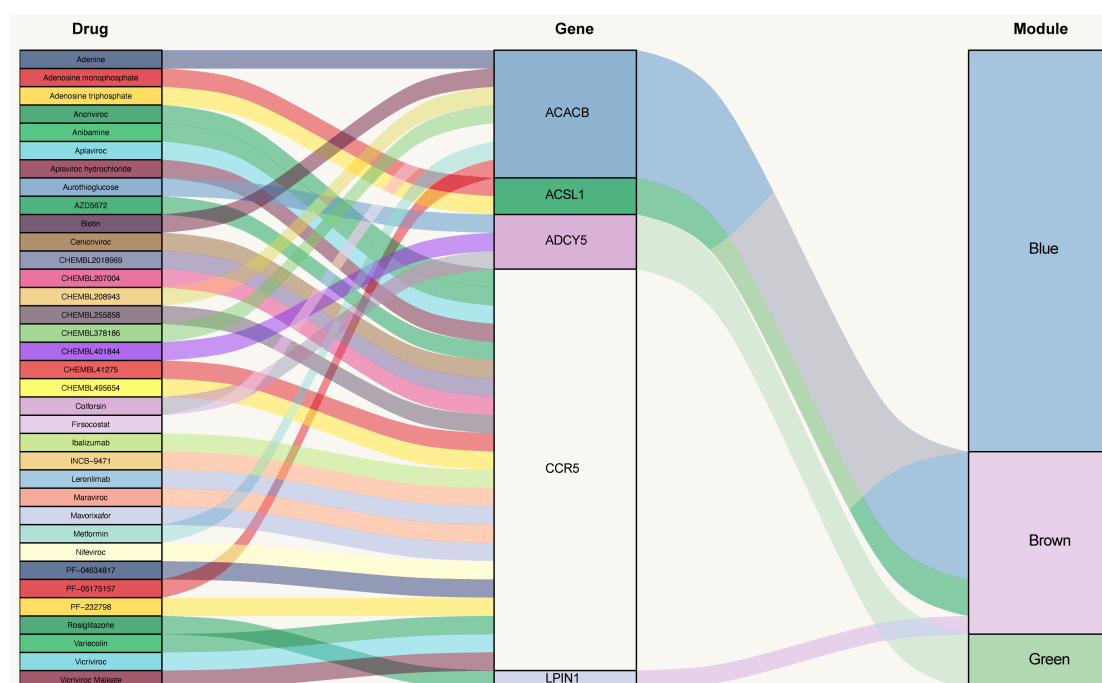


Figure 28. Gene-drug interaction prediction of key genes. Five key genes: ACACB, ACSL1, ADCY5, CCR5 and LPIN1 were targeted in the DGldb database. And a total of 35 potential target drugs/compounds were predicted from the database.

Table 9. Potential target agents identified based on drug-gene interaction in DGIdb database.

Gene symbol	Gene name	Target agent	Drug-gene Interaction	Query Score	Interaction Score
ACACB	Acetyl-CoA Carboxylase Beta	CHEMBL378186	NA	4.45	8.74
		Adenine	NA	4.45	8.74
		PF-05175157	NA	4.45	8.74
		CHEMBL208943	NA	4.45	8.74
		Firsocostat	Allosteric modulator	2.22	4.37
		Biotin	Cofactor	1.33	2.62
		Metformin	NA	0.11	0.22
ACSL1	Acyl-CoA Synthetase Long-Chain Family Member 1	Adenosine monophosphate	NA	0.89	6.12
		Adenosine triphosphate	NA	0.23	1.61
ADCY5	Adenylate Cyclase 5	CHEMBL401844	NA	2.22	10.2
		Aurothioglucose	NA	1.48	6.8
		Colforsin	NA	0.74	3.4
CCR5	C-C motif chemokine receptor 5	Maraviroc	Antagonist	31.15	19.47
CCR5	C-C motif chemokine receptor 5	Vicriviroc	Antagonist	26.7	16.69
		Leronlimab	Antagonist	22.25	13.91
		CHEMBL207004	Antagonist	17.8	11.13
		INCB-9471	Antagonist	13.35	8.34
		Cenicriviroc	Antagonist	8.9	5.56
		AZD5672	Antagonist	8.9	5.56
		Aplaviroc	Antagonist	8.9	5.56
		Ancriviroc	Antagonist	4.45	2.78
		Vicriviroc Maleate	Antagonist	4.45	2.78
		Anibamine	NA	4.45	2.78
		Variocolin	NA	4.45	2.78
		CHEMBL255858	NA	4.45	2.78
		CHEMBL495654	NA	4.45	2.78
		PF-232798	NA	4.45	2.78
		Nifeviroc	NA	4.45	2.78
		Aplaviroc hydrochloride	Antagonist	2.22	1.39
		CHEMBL41275	Antagonist	2.22	1.39
PF-04634817	Antagonist	2.22	1.39		
CHEMBL2018969	Antagonist	2.22	1.39		
Mavorixafor	NA	2.22	1.39		
Ibalizumab	Antagonist	1.11	0.7		
LPIN1	Lipin 1	Rosiglitazone	NA	0.28	3.82

4 DISCUSSION

4.1 Influence of blue light irradiation on endothelial cells

The purpose of this study was to systematically investigate the impact of LED blue light with a wavelength of 453 nm on HUVECs in vitro, including cell metabolism, proliferation, migration and angiogenic functions. Results showed that firstly blue light irradiation could influence the mentioned biological activities of HUVECs in vitro and yield a biphasic effect after light treatment. At a low fluence ($10 \text{ mW/cm}^2 * 12 \text{ min}$, 7.2 J/cm^2), blue light promoted cell metabolism, migration and angiogenic functions of HUVECs. However, at high fluence ($40 \text{ mW/cm}^2 * 12 \text{ min}$, 28.8 J/cm^2), blue light irradiation inhibited all the above-mentioned cell activities. Secondly, we found that blue light increased the intercellular ROS production in a fluence-dependent manner. Furthermore, we revealed the potential mechanisms of the observed biphasic effect by RNA sequencing. Several angiogenic related pathways, e.g., MAPK, JAK-STAT, PI3K-Akt and VEGF- which are known to improve cell viability and migration - were upregulated in the low fluence group, while Ferroptosis, Necroptosis and the p53 signaling pathways - which are known to regulate above cell activities negatively - were activated after higher fluences of light irradiation.

4.1.1 Inhibition phase of blue light on endothelial cells

The wavelength of blue light ranges from 380 nm to 500 nm. It possesses some ultraviolet properties, including the inhibitory effect on bacteria or eukaryotes, as the wavelength of ultraviolet is between 10nm and 400 nm ⁸⁵. These inhibition characteristics induced by blue light are now widely accepted in antimicrobial therapy. It was reported that blue light could target several bacterial species. For example, *Helicobacter pylori* (*H. pylori*), a gram-negative bacterium found in the human stomach that may lead to peptic ulcer and gastric cancer could be reduced by 99.9% after 20 J/cm^2 of blue light exposure (405 nm wavelength, 100 mW/cm^2 irradiance) ⁸⁶. Besides targeting gram-negative bacteria, gram-positive bacteria could also be targeted by blue light. Kawada et al. isolated five acne patient-derived strains of *Propionibacterium acnes* (*P. acnes*), a gram-positive bacterium that causes acne symptoms and antimicrobial resistance, to assess the bactericidal efficacy of blue light (407-420 nm wavelengths). With the exposure to blue light for 60 min with an irradiance of 90 mW/cm^2 (total influence 324 J/cm^2), the viability of *P. acnes* was

decreased by 15.7% immediately after the irradiation 24.4% at 60 min post-irradiation⁸⁷. In another study on blue light inactivation of oral bacteria *Porphyromonas gingivalis* (*P. gingivalis*), was targeted, a bacterium that may cause periodontal disease. Exposure to 15 J/cm² with the wavelength of 405 nm blue light lead to evident inhibition of *P. gingivalis* (over 75% inhibition) under different irradiation conditions of 50 mW/cm² for 300 s, 200 mW/cm² for 75 s and 400 mW/cm² for 38 s⁸⁸. Other strains of bacteria were also affected by blue light including *S. aureus* (405nm wavelength with 100 mW/cm² * 10 mins)⁸⁹ and *P. aeruginosa* (405nm wavelength with 5-15 J/cm²)⁹⁰. Both were reported to be inactivated by blue light irradiation. These studies illustrated the inhibitory role of blue light in the antimicrobial application.

In the field of cancer research, blue light also showed an inhibitory influence on tumor cells. In an in vitro study carried out by Yan et al., blue light (470 nm wavelength) induced lower cell proliferation and a remarkable increase of cell apoptosis of human colorectal cancer cell lines: SW620 and HT29, which were treated by 72 J/cm² to 288 J/cm². Meanwhile, the cell migration was significantly decreased after blue light irradiation, which further inhibited the epithelial-mesenchymal transition process⁹¹. In a similar study, cell viability of HT-29 and HCT-116, two other human colon cancer cells, was lower (around 10% with 10 mins at 30 mW/cm² and 60% with 30 mins at 30 mW/cm²) after irradiation by 456 nm blue light as compared to control group⁹². In an in vivo study of v-Ha-ras transgenic induced skin tumor models, blue light (470 nm wavelength at 5.7 mW/cm²) decreased the tumor incidence rate and tumor size after daily 1-hour irradiation over 9 weeks⁹³.

In our study, the inhibitory effect on HUVECs was observed when a higher fluence of blue light irradiation was applied (i.e., 453 nm wavelength with 12 mins at 40 mW/cm²). This is consistent with the results observed for other types of endothelial cells. Blue light (425-500 nm wavelength) significantly inhibits the cell growth of endothelial cells derived from the calf aortas exposed for 18 hours at 42 J/cm²⁹⁴. A study from Sparsa et al. showed the exposure of bovine endothelial cells to blue light (450 nm wavelength at 10 J/cm²) induced an apparent reduction in cell viability and an increase in cell death 24 hours after irradiation⁹⁵. However, one study reported that treatment with blue light (475 nm wavelength at 40 mW/cm², 24 J/cm² per day for 3 days) on HUCVECs was ineffective. There was no promotion of cell viability or cell migration which could be induced by blue light⁹⁶. This difference may come from the

parameters of irradiation like wavelength or the different sources of light which were used.

4.1.2 Mechanisms of inhibitory effect on endothelial cells after blue light irradiation

To reveal the potential underlying mechanisms of blue light-induced inhibition on HUVECs, we performed ROS measurements as the excess amount of cellular ROS leads to oxidation of proteins, nucleic acids, lipids, membranes and organelles, which induces programmed cell death^{82,97}. We also performed Gene expression profiling by RNA-seq to detect the transcriptomic changes after blue light irradiation.

Firstly, ROS level in HUVECs was significantly upregulated in the high fluence group after blue light irradiation as detected by a redox sensor and typical DCFH-DA staining.

We also observed consecutive increase of cell apoptosis detected by annexin-V and with PI staining. This is consistent with the results observed in several in vivo and in vitro studies. For instance, one study showed that dose-dependent ROS upregulation occurred both in normal (NHEK) and oral squamous carcinoma (OSC2) epithelial cells with blue light (380–500 nm wavelengths) irradiation doses of 5–30 J/cm²⁹⁷. Furthermore, blue light (470 nm wavelength) caused ROS accumulation and DNA damage in human colorectal cancer cell lines SW620 and HT29, which further induced a remarkable increase of cell apoptosis - which we also found in HUVECs. In parallel, the cell migration ability of these two tumor cells was affected⁹¹. King et al. provided details about how blue light related-ROS caused the cell death: they found that mitochondria-derived reactive oxygen species (ROS) are responsible for the death of retinal pigment epithelium exposed to blue light (425 nm wavelength at 10 mW/mm² for 5 mins), as both ROS production and cell death were decreased when they inhibited the mitochondrial electron transport chain or applied mitochondria-specific antioxidants to cells⁹⁸. In another in vivo study investigating oral gingival tissue exposed to blue light (460 nm wavelength at 400 mW/cm² for 15 mins), the oxidative stress caused by ROS and the oxidized glutathione levels were significantly increased. These effects could be inhibited by pre-administration of anti-oxidative stress reagent N-acetyl-L-cysteine (NAC), which provides the strategy against blue light-induced oxidative damage⁹⁹.

Based on the KEGG pathway enrichment analysis of RNA sequencing data from cells exposed to high fluences of blue light, we found apoptosis-related pathways-

Ferroptosis, Necroptosis and p53 pathways were upregulated. Ferroptosis is a nonapoptotic type of cell death initiated by the lipid peroxidation accumulation and iron metabolism derived from ROS overload ¹⁰⁰. It is characterized by smaller mitochondria with increased mitochondrial membrane densities, reduced mitochondria crista, and rupture of the outer mitochondrial membrane ¹⁰¹. Herein, ROS overproduction caused by the high fluence of blue light irradiation in this study would activate the Ferroptosis pathway and cause ferroptotic cell death in HUVECs. Necroptosis is another form of programmed cell death, mimicking some features of apoptosis and necrosis ¹⁰². A recent study in retinal cells found that blue light (450 nm wavelength at 300lux for 48 hours) induced cell necroptosis by activating the apoptosis-inducing factor (AIF) ¹⁰³. p53 pathway – as the last apoptotic related pathway - regulates the cell response to intrinsic and extrinsic stress including oxidative stress and DNA damage ¹⁰⁴. Both can be triggered by blue light irradiation. In this study, gene set enrichment analysis further proved the upregulation of this pathway.

QPCR validation of the p53 pathway showed that CASP9 and BAX were significantly upregulated in cells irradiated by high-fluence blue light. CASP9 encodes the Caspase-9 protease required for apoptosis ^{105,106} and BAX is an apoptosis regulator involved in the p53-regulated apoptosis ^{107,108}. Thus, the induction of blue light-mediated apoptosis may also explain the inhibitory effects observed for the cell behavior in the study (cell viability, migration and angiogenesis).

Besides the above three enriched pathways, metabolism-related pathways were the most prominent part in the results of KEGG pathway enrichment analysis, among which pathways of “Carbohydrate metabolism” and “Lipid metabolism” accounted for a larger proportion of total enriched pathways. At present no studies have been published showing that blue light would affect these above two pathways, carbohydrate or lipid metabolism plays a crucial role in regulating the biological activities of endothelial cells ¹⁴. For instance, inhibition of 6-phosphofructo-2-kinase/fructose-2,6-biphosphatase 3 (PFKFB3), a key enzyme in carbohydrate metabolism, would switch proliferating endothelial cells to a quiescent state, which further disturbs the cell migration and tube formation ^{109,110}. Dysregulation of fatty acid metabolism, one subtype of lipid metabolism, could disrupt the intercellular redox homeostasis, including oxidative stress regulation in endothelial cells, which leads to cell dysfunction and destruction of the vascular barrier ^{111,112}.

4.1.3 Promotion phase of blue light on endothelial cells

Our study revealed that low fluence (irradiance at 10 mW/cm² for 12 min) of blue light (453 nm wavelength) could positively regulate HUVECs' activities including migration and angiogenesis. These findings further support the application of blue light treatment in wound healing because the promotion effect of blue light has also been described in several in vivo studies about wound healing. For instance, after seven consecutive days of blue light irradiation (470 nm wavelength at 50 mW/cm² for 10 mins/day), it significantly decreased the size of circular excision wounds in rats compared to the non-irradiated controls ¹¹³. In another study, blue light (470 nm wavelength with influence 30J/cm² per day) has been shown to increase angiogenesis and promotes wound healing in an ischemia rodent flap model. The necrosis of the ischemic tissues was attenuated and the flaps showed a significantly increased tissue perfusion at day 7 in the blue LED-treated group ³⁸. In a clinical study about the effectiveness of blue light photobiomodulation in chronic wounds, 19 patients were enrolled and treated with a power density of 120mW/cm² and a fluence of 7.2 J/cm² of blue light. During the 10-week study, 84% of the patients responded to the treatment. Wounds were reduced with no signs of infection ¹¹⁴. Most recently, Stern et al. revealed that 30 mins of blue light (453 nm wavelength at 42 mW/cm²) treatment decreased the blood pressure by increasing NO-releasing into circulating blood in healthy volunteers, which d may also provide a novel field of application for blue light treatment.

4.1.4 Mechanisms of promotion effect on endothelial cells after blue light irradiation

In this study, four angiogenesis-related pathways- "JAK-STAT signaling pathway", "MAPK signaling pathway", "PI3K-Akt signaling pathway" and "VEGF signaling pathway" were upregulated in the KEGG pathway enrichment analysis, all of which may explain the promotion effects of low influence blue light irritation on cell viability, migration and angiogenesis. The JAK-STAT signaling pathway is essential for basic developmental processes including cell proliferation and differentiation ^{115,116}. Many studies have proved robust angiogenic effects of this pathway on endothelial cells. It mediates the cell degradation of the basement membrane and extracellular matrix proliferation, migration and proliferation during angiogenesis ¹¹⁷. MAPK signaling pathway is a pathway activated by pro-angiogenic factors FGF and VEGF, enhancing cell migration and proliferation in the early stages of angiogenesis ^{118,119}. The PI3K-

Akt signaling pathway and VEGF signaling pathway are the two well-known pathways regulating multiple cellular processes during angiogenesis^{120,121}. We found three genes in the VEGF pathway which were significantly increased and could be validated by qPCR analysis. The first gene is PTGS2, also known as cyclooxygenase-2 (COX-2). It has been reported to be involved in VEGF-mediated angiogenesis of HUVEC cells through activating the p38 MAPK and JNK kinase pathway¹⁰⁶. Interestingly, we also found these pathways to be upregulated in the KEGG enrichment analysis. The second upregulated gene, PLA2G4A (alias for cPLA2 gene) has so far no direct connection with blue light or angiogenesis. Only one study has indicated that cPLA2 was regulated by MAP kinase¹⁰⁵, which was found upregulated after low fluence irradiation.

The third upregulated gene is NOS3, nitric oxide synthase 3, which controls nitric oxide production (NO)¹²². Several studies have focused on nitric oxide production (NO) under blue light illumination, as NO plays a vital role in maintaining vascular homeostasis^{123,124}. One study showed blue light (420-453 nm wavelengths at 58 mW/cm²)-induced NO formation in human skin in vitro and in vivo¹²⁵. A recent clinical study showed that 30 mins of blue light (453 nm wavelength at 42 mW/cm²) treatment could promote NO-release into circulating blood followed by a decrease in blood pressure in healthy volunteers³⁹.

4.2 Weighted gene co-expression network analysis in the development of abdominal aortic aneurysm

The present work was published in *Biomedicines* 2021, 9(5), 546; <https://doi.org/10.3390/biomedicines9050546>.

4.2.1 Key modules of AAA progression

WGCNA is a systematic biological method that identifies the gene co-expression clusters among samples in an unbiased manner. This study used WGCNA analysis to identify the key gene clusters called modules involved in AAA progression. Among the 15 co-expression modules obtained by WGCNA analysis, the blue, green, and brown modules were most related to AAA progression. Based on the functional enrichment analysis of these key modules, we found genes in the blue module were mainly enriched in the cellular process, particularly the regulation of the mitotic cell cycle. The mitotic cell cycle is a process that proliferating cells go through a regular

cycle of events, which is also known as cell division ¹²⁶. There have been several studies to imply the association between the mitotic cell cycle and aortic diseases. The results from Butt et al. showed that significantly expressed genes in the peripheral blood between individuals with AAA and healthy organ donors were enriched in this process ¹²⁷. Another study showed that genes upregulated in acute type A aortic dissection, a disease that shares some similarities with AAA, significantly clustered in the biological process of the mitotic cell cycle ¹²⁸. The most enriched pathway of the blue module was fluid shear stress and atherosclerosis. This finding was consistent with several studies. Abnormal blood flow-induced shear stress was reported to contribute to the growth or rupture of AAA ^{129,130}. And the studies from Cornuz et al. and Golledge et al. revealed the potential connections between atherosclerosis and AAA development ^{42,131}. The GO analysis of the green module showed that the biological process of GTPase activity was involved in AAA development. It was reported that dysregulation of GTPase activity would affect the proliferation and migration of endothelial cells and vascular smooth cells, further leading to the AAA progression ^{132,133}. KEGG pathway enrichment of green module demonstrated that the regulation of lipolysis in adipocytes pathway might also be engaged in the growth of AAA, as some studies indicated the associations of lipolysis and adipocytes with AAA ^{134–136}. The functional enrichment analysis of the brown module revealed that some metabolic processes or pathways are also involved in AAA progression. Cofactor metabolism was the most enriched process in this study, which was in agreement with previous studies indicating that cofactors like cobalamin (vitamin B12) and glutathione could limit the progression of AAA ^{137,138}. These findings confirmed the involvement of the mitotic cell cycle, GTPase activity, and metabolic process in the pathogenesis of AAA. However, other GO analyses like organelle fission and purine-related metabolic process, pathways including pancreatic secretion, propanoate metabolism and pyruvate metabolism need further investigation in the future.

4.2.2 Hub genes related to AAA progression

In WGCNA analysis, hub genes are defined as genes with high correlation in candidate modules ⁶⁰. In our study, we selected the hub genes by a combined analysis of gene intramodular connectivity and protein-protein interaction in the STRING database and Cytoscape software. Then the chosen hub genes were further confirmed in mouse and human datasets through differential gene expression

analysis. Finally, we identified seven key genes: CCR5 from the blue module, ADCY5 and ADCY3 from the green module, ACACB, LPIN1, ACSL1, and UCP3 from the brown module. CCR5 was a member of C-C motif chemokine receptors, a key receptor during HIV-1 infection¹³⁹. It is expressed in many immune cells, including macrophages, T cells, and natural killer cells. CCR5 and its ligands regulate the inflammatory response by affecting the biological activities of the above-mentioned immune cells¹⁴⁰. The results from GSE12591 identified Ccr5 as a differential gene upregulated in the mouse aortas with aneurysms⁵⁸, and CCR5 signaling in the macrophages pathway was enriched by functional analyses of differential genes in GSE7084⁵⁷. Patients with AAA frequently had CCR5 Delta 32 deletion mutations and were vulnerable to rupture of aneurysms¹⁴¹. Thus, CCR5 may be a potential biomarker for the selection of AAA patients who need active intervention. The hub gene ADCY5 was one of the differential expression genes in the murine dissecting AAA¹⁴², so it may also play a role in the growth of AAA. ADCY3 is an enzyme that regulates cyclic adenosine monophosphate (cAMP). It was reported that loss of ADCY3 increased the risk of obesity and type 2 diabetes¹⁴³, and the single nucleotide polymorphisms of this gene are related to hypertension¹⁴⁴, which are the risk factors that may lead to AAA development. For the hub genes LPIN1, ACSL1 and UCP3, these three genes were related to adipocyte differentiation and muscle growth^{145–147}, so dysregulation of these genes may lead to AAA progression as adipocyte, and vascular smooth muscle cell play an essential role in the development of AAA^{135,148}. According to the reviewed literature, the remaining key gene ACACB had no apparent connection with AAA. This, however, requires further investigation to clarify its function in AAA progression.

4.2.3 Predicted drugs for AAA treatment

So far, there is no effective drug therapy for the prevention of AAA progression or rupture. Hence, we used seven identified key genes as drug targets for drug-gene interaction. A total of potential 35 drugs or compounds were predicted from the DGIdb database. We checked these 35 candidates from the literature and the ClinicalTrials.gov (<https://clinicaltrials.gov/>), the largest clinical trials database containing over 329,000 trials worldwide. Five targetable drugs (PF-05175157, firsocostat, and metformin targeting ACACB; maraviroc targeting CCR5; rosiglitazone targeting LPIN1) were found to be used for AAA treatment. PF-05175157 and firsocostat are two novel acetyl-CoA carboxylase (ACC) inhibitors for lipid disorder

(Alkhoury et al. 2020; Huard et al. 2020), which could potentially rebalance dysregulated lipid metabolism in AAA to limit the development of the disease. Metformin is the first-line oral antidiabetic drug, which had been proved to improve the prognosis of cardiovascular diseases by reducing inflammation and oxidative stress (Esfahanian et al. 2012; Isoda et al. 2006; S. A. Kim and Choi 2012). Several epidemiological studies have indicated that metformin use could decrease yearly AAA growth (Afonso et al. 2017; Francisci et al. 2019). Rosiglitazone (RGZ) is a potent peroxisome proliferator-activated receptor- γ (PPAR- γ) agonist that can protect against ischemia/reperfusion injury due to its anti-inflammatory effects (Yue Tian-li et al. 2001). It has been reported that RGZ reduces stent-induced neointimal formation by decreasing the inflammatory responses and vascular smooth muscle hyperplasia (Wu et al. 2017). It could also inhibit the growth and rupture of mouse aortic aneurysms induced by angiotensin II and high cholesterol through the same anti-inflammatory effect (Jones Alun et al. 2009). For the ADCY3 and UCP3 genes, no drugs were predicted to be evaluated as potential targets in AAA treatment in further studies.

5 SUMMARY

5.1 Influence of blue light irradiation on endothelial cells

Blue light irradiation at 453 nm regulated cell biological activities of HUVCEs, including cell metabolism, proliferation, migration and angiogenic functions. With low fluence light treatment, cell viability, migration, and angiogenesis were promoted by activation of related angiogenic pathways, especially the VEGF pathway.

In contrast, high fluence blue light irradiation showed the opposite effect on the above-mentioned cell activities. This inhibition was mediated through the upregulation of apoptosis and the p53 signaling pathways. From the data of our study, it can be speculated that blue light should be applied for wound healing especially in limb ischemia since it may enhance local angiogenesis if used at low fluence. In further studies, we will investigate if the inhibitory part of blue light may be used for the treatment of hemangioma or melanoma by suppressing or even reducing angiogenesis.

5.2 Weighted gene co-expression network analysis in the development of abdominal aortic aneurysm

Our study using WGCNA analyses identified seven key genes (CCR5, ADCY5, ADCY3, ACACB, LPIN1, ACSL1, UCP3) in three modules correlated to AAA progression. From the functional enrichment analysis, the Mitotic cell cycle, GTPase activity, and metabolic process were involved in the pathogenesis of AAA. The therapeutic potential of several predicted drugs for the treatment of AAA could be further explored.

6 REFERENCES

1. Carmeliet P, Jain RK. Molecular mechanisms and clinical applications of angiogenesis. *Nature*. 2011;473(7347):298-307. doi:10.1038/nature10144
2. Carmeliet P. Angiogenesis in health and disease. *Nature Medicine*. 2003;9(6):653-660. doi:10.1038/nm0603-653
3. Salamone M, Carfi Pavia F, Gherzi G. Proteolytic Enzymes Clustered in Specialized Plasma-Membrane Domains Drive Endothelial Cells' Migration. *PLoS One*. 2016;11(5). doi:10.1371/journal.pone.0154709
4. Andrée B, Ichanti H, Kalies S, et al. Formation of three-dimensional tubular endothelial cell networks under defined serum-free cell culture conditions in human collagen hydrogels. *Sci Rep*. 2019;9(1):5437. doi:10.1038/s41598-019-41985-6
5. Wanjare M, Kusuma S, Gerecht S. Perivascular cells in blood vessel regeneration. *Biotechnol J*. 2013;8(4):434-447. doi:10.1002/biot.201200199
6. Laakkonen JP, Lähteenvuo J, Jauhiainen S, Heikura T, Ylä-Herttuala S. Beyond endothelial cells: Vascular endothelial growth factors in heart, vascular anomalies and placenta. *Vascul Pharmacol*. 2019;112:91-101. doi:10.1016/j.vph.2018.10.005
7. Meyer RD, Mohammadi M, Rahimi N. A single amino acid substitution in the activation loop defines the decoy characteristic of VEGFR-1/FLT-1. *J Biol Chem*. 2006;281(2):867-875. doi:10.1074/jbc.M506454200
8. Jakobsson L, Franco CA, Bentley K, et al. Endothelial cells dynamically compete for the tip cell position during angiogenic sprouting. *Nat Cell Biol*. 2010;12(10):943-953. doi:10.1038/ncb2103
9. Abhinand CS, Raju R, Soumya SJ, Arya PS, Sudhakaran PR. VEGF-A/VEGFR2 signaling network in endothelial cells relevant to angiogenesis. *J Cell Commun Signal*. 2016;10(4):347-354. doi:10.1007/s12079-016-0352-8
10. Haigh JJ. Role of VEGF in organogenesis. *Organogenesis*. 2008;4(4):247-256.
11. Shibuya M. Vascular Endothelial Growth Factor (VEGF) and Its Receptor (VEGFR) Signaling in Angiogenesis. *Genes Cancer*. 2011;2(12):1097-1105. doi:10.1177/1947601911423031

12. Carmeliet P, Ferreira V, Breier G, et al. Abnormal blood vessel development and lethality in embryos lacking a single VEGF allele. *Nature*. 1996;380(6573):435-439. doi:10.1038/380435a0
13. Yancopoulos GD, Davis S, Gale NW, Rudge JS, Wiegand SJ, Holash J. Vascular-specific growth factors and blood vessel formation. *Nature*. 2000;407(6801):242-248. doi:10.1038/35025215
14. Li X, Sun X, Carmeliet P. Hallmarks of Endothelial Cell Metabolism in Health and Disease. *Cell Metabolism*. 2019;30(3):414-433. doi:10.1016/j.cmet.2019.08.011
15. Culic O, Gruwel ML, Schrader J. Energy turnover of vascular endothelial cells. *Am J Physiol*. 1997;273(1 Pt 1):C205-213. doi:10.1152/ajpcell.1997.273.1.C205
16. Krützfeldt A, Spahr R, Mertens S, Siegmund B, Piper HM. Metabolism of exogenous substrates by coronary endothelial cells in culture. *Journal of Molecular and Cellular Cardiology*. 1990;22(12):1393-1404. doi:10.1016/0022-2828(90)90984-A
17. Potente M, Gerhardt H, Carmeliet P. Basic and therapeutic aspects of angiogenesis. *Cell*. 2011;146(6):873-887. doi:10.1016/j.cell.2011.08.039
18. De Bock K, Georgiadou M, Schoors S, et al. Role of PFKFB3-driven glycolysis in vessel sprouting. *Cell*. 2013;154(3):651-663. doi:10.1016/j.cell.2013.06.037
19. Parra-Bonilla G, Alvarez DF, Al-Mehdi A-B, Alexeyev M, Stevens T. Critical role for lactate dehydrogenase A in aerobic glycolysis that sustains pulmonary microvascular endothelial cell proliferation. *Am J Physiol Lung Cell Mol Physiol*. 2010;299(4):L513-522. doi:10.1152/ajplung.00274.2009
20. Peters K, Kamp G, Berz A, et al. Changes in human endothelial cell energy metabolic capacities during in vitro cultivation. The role of “aerobic glycolysis” and proliferation. *Cell Physiol Biochem*. 2009;24(5-6):483-492. doi:10.1159/000257490
21. Talley JT, Mohiuddin SS. Biochemistry, Fatty Acid Oxidation. In: *StatPearls*. StatPearls Publishing; 2021. Accessed May 20, 2021. <http://www.ncbi.nlm.nih.gov/books/NBK556002/>
22. Schoors S, Bruning U, Missiaen R, et al. Fatty acid carbon is essential for dNTP synthesis in endothelial cells. *Nature*. 2015;520(7546):192-197. doi:10.1038/nature14362
23. Huang H, Vandekeere S, Kalucka J, et al. Role of glutamine and interlinked asparagine metabolism in vessel formation. *EMBO J*. 2017;36(16):2334-2352. doi:10.15252/embj.201695518

24. Wang M, Rao J, Wang M, et al. Cancer photo-immunotherapy: from bench to bedside. *Theranostics*. 2021;11(5):2218-2231. doi:10.7150/thno.53056
25. Nomura S, Morimoto Y, Tsujimoto H, et al. Highly reliable, targeted photothermal cancer therapy combined with thermal dosimetry using a near-infrared absorbent. *Scientific Reports*. 2020;10(1):9765. doi:10.1038/s41598-020-66646-x
26. Schultz DM, Yoon TP. Solar synthesis: prospects in visible light photocatalysis. *Science*. 2014;343(6174):1239176. doi:10.1126/science.1239176
27. Pulli T, Dönsberg T, Poikonen T, Manoocheri F, Kärhä P, Ikonen E. Advantages of white LED lamps and new detector technology in photometry. *Light: Science & Applications*. 2015;4(9):e332-e332. doi:10.1038/lisa.2015.105
28. Dong J, Xiong D. Applications of Light Emitting Diodes in Health Care. *Ann Biomed Eng*. 2017;45(11):2509-2523. doi:10.1007/s10439-017-1930-5
29. Guffey JS, Wilborn J. In Vitro Bactericidal Effects of 405-nm and 470-nm Blue Light. *Photomedicine and Laser Surgery*. 2006;24(6):684-688. doi:10.1089/pho.2006.24.684
30. E S, E Y, S G, Ar S, WI L. Anti-inflammatory properties of narrow-band blue light. *J Drugs Dermatol*. 2006;5(7):605-610.
31. Omi T, Bjerring P, Sato S, Kawana S, Hankins R, Honda M. 420 nm intense continuous light therapy for acne. *Journal of Cosmetic and Laser Therapy*. 2004;6(3):156-162. doi:10.1080/14764170410023785
32. Pfaff S, Liebmann J, Born M, Merk HF, von Felbert V. Prospective Randomized Long-Term Study on the Efficacy and Safety of UV-Free Blue Light for Treating Mild Psoriasis Vulgaris. *Dermatology*. 2015;231(1):24-34. doi:10.1159/000430495
33. Kumar P, Chawla D, Deorari A. Light-emitting diode phototherapy for unconjugated hyperbilirubinaemia in neonates. *Cochrane Database Syst Rev*. 2011;(12):CD007969. doi:10.1002/14651858.CD007969.pub2
34. Kaw U, Ilyas M, Bullock T, et al. A regimen to minimize pain during blue light photodynamic therapy of actinic keratoses: Bilaterally controlled, randomized trial of simultaneous versus conventional illumination. *Journal of the American Academy of Dermatology*. 2020;82(4):862-868. doi:10.1016/j.jaad.2019.09.010
35. Ramachandran A. Neonatal hyperbilirubinaemia. *Paediatrics and Child Health*. 2016;26(4):162-168. doi:10.1016/j.paed.2015.12.002

36. Maisels MJ, McDonagh AF. Phototherapy for Neonatal Jaundice. *New England Journal of Medicine*. 2008;358(9):920-928. doi:10.1056/NEJMct0708376
37. Genina EA, Titorenko VA, Belikov AV, Bashkatov AN, Tuchin VV. Adjunctive dental therapy via tooth plaque reduction and gingivitis treatment by blue light-emitting diodes tooth brushing. *J Biomed Opt*. 2015;20(12):128004. doi:10.1117/1.JBO.20.12.128004
38. Dungal P, Hartinger J, Chaudary S, et al. Low level light therapy by LED of different wavelength induces angiogenesis and improves ischemic wound healing. *Lasers Surg Med*. 2014;46(10):773-780. doi:10.1002/lsm.22299
39. Stern M, Broja M, Sansone R, et al. Blue light exposure decreases systolic blood pressure, arterial stiffness, and improves endothelial function in humans. *European Journal of Preventive Cardiology*. 2018;25(17):1875-1883. doi:10.1177/2047487318800072
40. Rohringer S, Holnthoner W, Chaudary S, et al. The impact of wavelengths of LED light-therapy on endothelial cells. *Sci Rep*. 2017;7(1):10700. doi:10.1038/s41598-017-11061-y
41. Dorey CK, Delori FC, Akeo K. Growth of cultured RPE and endothelial cells is inhibited by blue light but not green or red light. *Current Eye Research*. Published online July 2, 2009. doi:10.3109/02713689008999595
42. Golledge J, Muller J, Daugherty A, Norman P. Abdominal aortic aneurysm: pathogenesis and implications for management. *Arterioscler Thromb Vasc Biol*. 2006;26(12):2605-2613. doi:10.1161/01.ATV.0000245819.32762.cb
43. GBD 2013 Mortality and Causes of Death Collaborators. Global, regional, and national age-sex specific all-cause and cause-specific mortality for 240 causes of death, 1990-2013: a systematic analysis for the Global Burden of Disease Study 2013. *Lancet*. 2015;385(9963):117-171. doi:10.1016/S0140-6736(14)61682-2
44. Sampson UKA, Norman PE, Fowkes FGR, et al. Global and regional burden of aortic dissection and aneurysms: mortality trends in 21 world regions, 1990 to 2010. *Glob Heart*. 2014;9(1):171-180.e10. doi:10.1016/j.ghart.2013.12.010
45. Toghiani BJ, Saratzis A, Bown MJ. Abdominal aortic aneurysm—an independent disease to atherosclerosis? *Cardiovascular Pathology*. 2017;27:71-75. doi:10.1016/j.carpath.2017.01.008
46. Wanhainen A, Verzini F, Van Herzele I, et al. Editor's Choice - European Society for Vascular Surgery (ESVS) 2019 Clinical Practice Guidelines on the

Management of Abdominal Aorto-iliac Artery Aneurysms. *Eur J Vasc Endovasc Surg.* 2019;57(1):8-93. doi:10.1016/j.ejvs.2018.09.020

47. Dua A, Kuy S, Lee CJ, Upchurch GR, Desai SS. Epidemiology of aortic aneurysm repair in the United States from 2000 to 2010. *Journal of Vascular Surgery.* 2014;59(6):1512-1517. doi:10.1016/j.jvs.2014.01.007

48. Schermerhorn ML, Bensley RP, Giles KA, et al. Changes in Abdominal Aortic Aneurysm Rupture and Short Term Mortality 1995–2008. *Ann Surg.* 2012;256(4):651-658. doi:10.1097/SLA.0b013e31826b4f91

49. Blankensteijn JD, de Jong SECA, Prinssen M, et al. Two-year outcomes after conventional or endovascular repair of abdominal aortic aneurysms. *N Engl J Med.* 2005;352(23):2398-2405. doi:10.1056/NEJMoa051255

50. Tonnessen BH, Sternbergh WC, Money SR. Mid- and long-term device migration after endovascular abdominal aortic aneurysm repair: a comparison of AneuRx and Zenith endografts. *J Vasc Surg.* 2005;42(3):392-400; discussion 400-401. doi:10.1016/j.jvs.2005.05.040

51. Chaikof EL, Dalman RL, Eskandari MK, et al. The Society for Vascular Surgery practice guidelines on the care of patients with an abdominal aortic aneurysm. *J Vasc Surg.* 2018;67(1):2-77.e2. doi:10.1016/j.jvs.2017.10.044

52. Kokje VBC, Hamming JF, Lindeman JHN. Pharmaceutical Management of Small Abdominal Aortic Aneurysms: A Systematic Review of the Clinical Evidence. *Journal of Vascular Surgery.* 2015;62(6):1680. doi:10.1016/j.jvs.2015.10.080

53. Rughani G, Robertson L, Clarke M. Medical treatment for small abdominal aortic aneurysms. *Cochrane Database Syst Rev.* 2012;(9):CD009536. doi:10.1002/14651858.CD009536.pub2

54. Kuivaniemi H, Ryer EJ, Elmore JR, Tromp G. Understanding the pathogenesis of abdominal aortic aneurysms. *Expert Review of Cardiovascular Therapy.* 2015;13(9):975-987. doi:10.1586/14779072.2015.1074861

55. Raffort J, Lareyre F, Clément M, Hassen-Khodja R, Chinetti G, Mallat Z. Monocytes and macrophages in abdominal aortic aneurysm. *Nature Reviews Cardiology.* 2017;14(8):457-471. doi:10.1038/nrcardio.2017.52

56. Weintraub NL. Understanding Abdominal Aortic Aneurysm. *New England Journal of Medicine.* 2009;361(11):1114-1116. doi:10.1056/NEJMcibr0905244

57. Pahl MC, Erdman R, Kuivaniemi H, Lillvis JH, Elmore JR, Tromp G. Transcriptional (ChIP-Chip) Analysis of ELF1, ETS2, RUNX1 and STAT5 in Human

Abdominal Aortic Aneurysm. *Int J Mol Sci*. 2015;16(5):11229-11258.

doi:10.3390/ijms160511229

58. Rush C, Nyara M, Moxon JV, Trollope A, Cullen B, Golledge J. Whole genome expression analysis within the angiotensin II-apolipoprotein E deficient mouse model of abdominal aortic aneurysm. *BMC Genomics*. 2009;10:298. doi:10.1186/1471-2164-10-298

59. Spin JM, Hsu M, Azuma J, et al. Transcriptional profiling and network analysis of the murine angiotensin II-induced abdominal aortic aneurysm. *Physiol Genomics*. 2011;43(17):993-1003. doi:10.1152/physiolgenomics.00044.2011

60. Zhang B, Horvath S. A General Framework for Weighted Gene Co-Expression Network Analysis. *Statistical Applications in Genetics and Molecular Biology*. 2005;4(1). doi:10.2202/1544-6115.1128

61. Guo N, Zhang N, Yan L, et al. Weighted gene co-expression network analysis in identification of key genes and networks for ischemic-reperfusion remodeling myocardium. *Mol Med Rep*. 2018;18(2):1955-1962. doi:10.3892/mmr.2018.9161

62. Nagenborg J, Jin H, Brennan E, Goossens P, Donners M, Biessen E. Re-Programming Atherosclerotic Plaque Macrophages Towards An Anti-Atherogenic Phenotype. *Atherosclerosis*. 2019;287:e79. doi:10.1016/j.atherosclerosis.2019.06.228

63. Wang C, Shi H, Chen L, Li X, Cao G, Hu X. Identification of Key lncRNAs Associated With Atherosclerosis Progression Based on Public Datasets. *Front Genet*. 2019;10. doi:10.3389/fgene.2019.00123

64. Langfelder P, Horvath S. WGCNA: an R package for weighted correlation network analysis. *BMC Bioinformatics*. 2008;9(1):559. doi:10.1186/1471-2105-9-559

65. Jaffe EA, Nachman RL, Becker CG, Minick CR. Culture of Human Endothelial Cells Derived from Umbilical Veins. IDENTIFICATION BY MORPHOLOGIC AND IMMUNOLOGIC CRITERIA. *J Clin Invest*. 1973;52(11):2745-2756.

66. Gutscher M, Pauleau A-L, Marty L, et al. Real-time imaging of the intracellular glutathione redox potential. *Nat Methods*. 2008;5(6):553-559. doi:10.1038/nmeth.1212

67. C D, K P, G B, et al. High-level transduction and gene expression in hematopoietic repopulating cells using a human immunodeficiency [correction of imunodeficiency] virus type 1-based lentiviral vector containing an internal spleen

focus forming virus promoter. *Hum Gene Ther.* 2002;13(7):803-813.

doi:10.1089/10430340252898984

68. Foty R. A Simple Hanging Drop Cell Culture Protocol for Generation of 3D Spheroids. *J Vis Exp.* 2011;(51). doi:10.3791/2720

69. Biros E, Gäbel G, Moran CS, et al. Differential gene expression in human abdominal aortic aneurysm and aortic occlusive disease. *Oncotarget.*

2015;6(15):12984-12996. doi:10.18632/oncotarget.3848

70. Ritchie ME, Phipson B, Wu D, et al. limma powers differential expression analyses for RNA-sequencing and microarray studies. *Nucleic Acids Res.*

2015;43(7):e47-e47. doi:10.1093/nar/gkv007

71. Kassambara A. *Ggcorrplot: Visualization of a Correlation Matrix Using*

“Ggplot2.”; 2019. Accessed September 30, 2020. [https://CRAN.R-](https://CRAN.R-project.org/package=ggcorrplot)

[project.org/package=ggcorrplot](https://CRAN.R-project.org/package=ggcorrplot)

72. Yu G, Wang L-G, Han Y, He Q-Y. clusterProfiler: an R Package for Comparing Biological Themes Among Gene Clusters. *OMICS: A Journal of Integrative Biology.*

2012;16(5):284-287. doi:10.1089/omi.2011.0118

73. Szklarczyk D, Morris JH, Cook H, et al. The STRING database in 2017: quality-controlled protein–protein association networks, made broadly accessible.

Nucleic Acids Res. 2017;45(D1):D362-D368. doi:10.1093/nar/gkw937

74. Shannon P, Markiel A, Ozier O, et al. Cytoscape: A Software Environment for Integrated Models of Biomolecular Interaction Networks. *Genome Res.*

2003;13(11):2498-2504. doi:10.1101/gr.1239303

75. Chin C-H, Chen S-H, Wu H-H, Ho C-W, Ko M-T, Lin C-Y. cytoHubba:

identifying hub objects and sub-networks from complex interactome. *BMC Syst Biol.*

2014;8(4):S11. doi:10.1186/1752-0509-8-S4-S11

76. Cotto KC, Wagner AH, Feng Y-Y, et al. DGIdb 3.0: a redesign and expansion of the drug–gene interaction database. *Nucleic Acids Res.* 2018;46(D1):D1068-

D1073. doi:10.1093/nar/gkx1143

77. Wickham H, Chang W, Henry L, et al. *Ggplot2: Create Elegant Data*

Visualisations Using the Grammar of Graphics.; 2020. Accessed April 12, 2020.

<https://CRAN.R-project.org/package=ggplot2>

78. Brunson JC. *Ggalluvial: Alluvial Plots in “Ggplot2.”*; 2019. Accessed April 12,

2020. <https://CRAN.R-project.org/package=ggalluvial>

79. Becker A, Distler E, Klapczynski A, et al. Blue light inhibits proliferation of melanoma cells. In: *Mechanisms of Photobiomodulation Therapy XI*. Vol 9695. International Society for Optics and Photonics; 2016:969503. doi:10.1117/12.2209504
80. Becker A, Sticht C, Dweep H, Abeelen FA van, Gretz N, Oversluizen G. Impact of blue LED irradiation on proliferation and gene expression of cultured human keratinocytes. In: *Mechanisms for Low-Light Therapy X*. Vol 9309. International Society for Optics and Photonics; 2015:930909. doi:10.1117/12.2083010
81. Becker A, Klapczynski A, Kuch N, et al. Gene expression profiling reveals aryl hydrocarbon receptor as a possible target for photobiomodulation when using blue light. *Sci Rep*. 2016;6. doi:10.1038/srep33847
82. El-Esawi M, Arthaut L-D, Jourdan N, et al. Blue-light induced biosynthesis of ROS contributes to the signaling mechanism of Arabidopsis cryptochrome. *Scientific Reports*. 2017;7(1):13875. doi:10.1038/s41598-017-13832-z
83. Lockwood DB, Wataha JC, Lewis JB, Tseng WY, Messer RLW, Hsu SD. Blue light generates reactive oxygen species (ROS) differentially in tumor vs. normal epithelial cells. *Dent Mater*. 2005;21(7):683-688. doi:10.1016/j.dental.2004.07.022
84. Ryter SW, Kim HP, Hoetzel A, et al. Mechanisms of cell death in oxidative stress. *Antioxid Redox Signal*. 2007;9(1):49-89. doi:10.1089/ars.2007.9.49
85. Kleinpenning MM, Smits T, Frunt MHA, van Erp PEJ, van de Kerkhof PCM, Gerritsen RMJP. Clinical and histological effects of blue light on normal skin. *Photodermatol Photoimmunol Photomed*. 2010;26(1):16-21. doi:10.1111/j.1600-0781.2009.00474.x
86. Hamblin MR, Viveiros J, Yang C, Ahmadi A, Ganz RA, Tolkoff MJ. Helicobacter pylori accumulates photoactive porphyrins and is killed by visible light. *Antimicrob Agents Chemother*. 2005;49(7):2822-2827. doi:10.1128/AAC.49.7.2822-2827.2005
87. Kawada A, Aragane Y, Kameyama H, Sangen Y, Tezuka T. Acne phototherapy with a high-intensity, enhanced, narrow-band, blue light source: an open study and in vitro investigation. *J Dermatol Sci*. 2002;30(2):129-135. doi:10.1016/s0923-1811(02)00068-3
88. Fukui M, Yoshioka M, Satomura K, Nakanishi H, Nagayama M. Specific-wavelength visible light irradiation inhibits bacterial growth of Porphyromonas

- gingivalis. *J Periodontal Res.* 2008;43(2):174-178. doi:10.1111/j.1600-0765.2007.01009.x
89. Enwemeka CS, Williams D, Hollosi S, Yens D, Enwemeka SK. Visible 405 nm SLD light photo-destroys methicillin-resistant *Staphylococcus aureus* (MRSA) in vitro. *Lasers Surg Med.* 2008;40(10):734-737. doi:10.1002/lsm.20724
90. Guffey JS, Wilborn J. In vitro bactericidal effects of 405-nm and 470-nm blue light. *Photomed Laser Surg.* 2006;24(6):684-688. doi:10.1089/pho.2006.24.684
91. Yan G, Zhang L, Feng C, et al. Blue light emitting diodes irradiation causes cell death in colorectal cancer by inducing ROS production and DNA damage. *The International Journal of Biochemistry & Cell Biology.* 2018;103:81-88. doi:10.1016/j.biocel.2018.08.006
92. Yoshimoto T, Morine Y, Takasu C, et al. Blue light-emitting diodes induce autophagy in colon cancer cells by Opsin 3. *Annals of Gastroenterological Surgery.* 2018;2(2):154-161. doi:10.1002/ags3.12055
93. Ohara M, Kawashima Y, Kitajima S, Mitsuoka C, Watanabe H. Blue light inhibits the growth of skin tumors in the v-Ha-ras transgenic mouse. *Cancer Science.* 2003;94(2):205-209. doi:10.1111/j.1349-7006.2003.tb01420.x
94. Dorey CK, Delori FC, Akeo K. Growth of cultured RPE and endothelial cells is inhibited by blue light but not green or red light. *Current Eye Research.* 1990;9(6):549-559. doi:10.3109/02713689008999595
95. Sparsa A, Faucher K, Sol V, et al. Blue Light is Phototoxic for B16F10 Murine Melanoma and Bovine Endothelial Cell Lines by Direct Cytocidal Effect. *Anticancer Research.* 2010;30(1):143-147.
96. Rohringer S, Holnthoner W, Chaudary S, et al. The impact of wavelengths of LED light-therapy on endothelial cells. *Sci Rep.* 2017;7(1):10700. doi:10.1038/s41598-017-11061-y
97. Lockwood DB, Wataha JC, Lewis JB, Tseng WY, Messer RLW, Hsu SD. Blue light generates reactive oxygen species (ROS) differentially in tumor vs. normal epithelial cells. *Dental Materials.* 2005;21(7):683-688. doi:10.1016/j.dental.2004.07.022
98. King A, Gottlieb E, Brooks DG, Murphy MP, Dunaief JL. Mitochondria-derived Reactive Oxygen Species Mediate Blue Light-induced Death of Retinal Pigment Epithelial Cells¶. *Photochemistry and Photobiology.* 2004;79(5):470-475. doi:10.1111/j.1751-1097.2004.tb00036.x

99. Yoshida A, Shiotsu-Ogura Y, Wada-Takahashi S, Takahashi S, Toyama T, Yoshino F. Blue light irradiation-induced oxidative stress in vivo via ROS generation in rat gingival tissue. *Journal of Photochemistry and Photobiology B: Biology*. 2015;151:48-53. doi:10.1016/j.jphotobiol.2015.07.001
100. Xie Y, Hou W, Song X, et al. Ferroptosis: process and function. *Cell Death Differ*. 2016;23(3):369-379. doi:10.1038/cdd.2015.158
101. Galluzzi L, Vitale I, Abrams JM, et al. Molecular definitions of cell death subroutines: recommendations of the Nomenclature Committee on Cell Death 2012. *Cell Death Differ*. 2012;19(1):107-120. doi:10.1038/cdd.2011.96
102. Dhuriya YK, Sharma D. Necroptosis: a regulated inflammatory mode of cell death. *Journal of Neuroinflammation*. 2018;15(1):199. doi:10.1186/s12974-018-1235-0
103. Yang D, Rong R, Yang R, et al. CaMK II -induced Drp1 phosphorylation contributes to blue light-induced AIF-mediated necroptosis in retinal R28 cells. *Biochemical and Biophysical Research Communications*. 2021;559:113-120. doi:10.1016/j.bbrc.2021.04.082
104. Harris SL, Levine AJ. The p53 pathway: positive and negative feedback loops. *Oncogene*. 2005;24(17):2899-2908. doi:10.1038/sj.onc.1208615
105. Lin L-L, Wartmann M, Lin AY, Knopf JL, Seth A, Davis RJ. cPLA2 is phosphorylated and activated by MAP kinase. *Cell*. 1993;72(2):269-278. doi:10.1016/0092-8674(93)90666-E
106. Wu G, Luo J, Rana JS, Laham R, Sellke FW, Li J. Involvement of COX-2 in VEGF-induced angiogenesis via P38 and JNK pathways in vascular endothelial cells. *Cardiovascular Research*. 2006;69(2):512-519. doi:10.1016/j.cardiores.2005.09.019
107. Pawlowski J, Kraft AS. Bax-induced apoptotic cell death. *Proc Natl Acad Sci U S A*. 2000;97(2):529-531. doi:10.1073/pnas.97.2.529
108. Westphal D, Kluck RM, Dewson G. Building blocks of the apoptotic pore: how Bax and Bak are activated and oligomerize during apoptosis. *Cell Death Differ*. 2014;21(2):196-205. doi:10.1038/cdd.2013.139
109. De Bock K, Georgiadou M, Schoors S, et al. Role of PFKFB3-Driven Glycolysis in Vessel Sprouting. *Cell*. 2013;154(3):651-663. doi:10.1016/j.cell.2013.06.037
110. Vizán P, Sánchez-Tena S, Alcarraz-Vizán G, et al. Characterization of the metabolic changes underlying growth factor angiogenic activation: identification of

- new potential therapeutic targets. *Carcinogenesis*. 2009;30(6):946-952.
doi:10.1093/carcin/bgp083
111. Kalucka J, Bierhansl L, Conchinha NV, et al. Quiescent Endothelial Cells Upregulate Fatty Acid β -Oxidation for Vasculoprotection via Redox Homeostasis. *Cell Metabolism*. 2018;28(6):881-894.e13. doi:10.1016/j.cmet.2018.07.016
112. Patella F, Schug ZT, Persi E, et al. Proteomics-Based Metabolic Modeling Reveals That Fatty Acid Oxidation (FAO) Controls Endothelial Cell (EC) Permeability*[S]. *Molecular & Cellular Proteomics*. 2015;14(3):621-634.
doi:10.1074/mcp.M114.045575
113. Adamskaya N, Dungal P, Mittermayr R, et al. Light therapy by blue LED improves wound healing in an excision model in rats. *Injury*. 2011;42(9):917-921.
doi:10.1016/j.injury.2010.03.023
114. Marchelli M, Perniciaro G, Granara D, et al. Photobiomodulation with Blue Light in non-healing wounds: case series evaluation. 2019;10(3):4.
115. Amoyel M, Anderson AM, Bach EA. JAK/STAT pathway dysregulation in tumors: a Drosophila perspective. *Semin Cell Dev Biol*. 2014;28:96-103.
doi:10.1016/j.semcdb.2014.03.023
116. Arbouzova NI, Zeidler MP. JAK/STAT signalling in Drosophila: insights into conserved regulatory and cellular functions. *Development*. 2006;133(14):2605-2616.
doi:10.1242/dev.02411
117. Carmeliet P, Jain RK. Molecular mechanisms and clinical applications of angiogenesis. *Nature*. 2011;473(7347):298-307. doi:10.1038/nature10144
118. Song M, Finley SD. Mechanistic insight into activation of MAPK signaling by pro-angiogenic factors. *BMC Systems Biology*. 2018;12(1):145. doi:10.1186/s12918-018-0668-5
119. Tan WH, Popel AS, Gabhann FM. Computational Model of Gab1/2-Dependent VEGFR2 Pathway to Akt Activation. *PLOS ONE*. 2013;8(6):e67438.
doi:10.1371/journal.pone.0067438
120. Bader AG, Kang S, Zhao L, Vogt PK. Oncogenic PI3K deregulates transcription and translation. *Nat Rev Cancer*. 2005;5(12):921-929.
doi:10.1038/nrc1753
121. Karar J, Maity A. PI3K/AKT/mTOR Pathway in Angiogenesis. *Front Mol Neurosci*. 2011;4. doi:10.3389/fnmol.2011.00051

122. Oliveira-Paula GH, Lacchini R, Tanus-Santos JE. Endothelial nitric oxide synthase: from biochemistry and gene structure to clinical implications of NOS3 polymorphisms. *Gene*. 2016;575(2 Pt 3):584-599. doi:10.1016/j.gene.2015.09.061
123. Cooke JP. NO and angiogenesis. *Atheroscler Suppl*. 2003;4(4):53-60. doi:10.1016/s1567-5688(03)00034-5
124. Förstermann U, Münzel T. Endothelial nitric oxide synthase in vascular disease: from marvel to menace. *Circulation*. 2006;113(13):1708-1714. doi:10.1161/CIRCULATIONAHA.105.602532
125. Opländer C, Deck A, Volkmar CM, et al. Mechanism and biological relevance of blue-light (420-453 nm)-induced nonenzymatic nitric oxide generation from photolabile nitric oxide derivatives in human skin in vitro and in vivo. *Free Radic Biol Med*. 2013;65:1363-1377. doi:10.1016/j.freeradbiomed.2013.09.022
126. Miller OJ, Therman E. The Mitotic Cell Cycle. In: Miller OJ, Therman E, eds. *Human Chromosomes*. Springer; 2001:13-27. doi:10.1007/978-1-4613-0139-4_2
127. Butt HZ, Sylvius N, Salem MK, et al. Microarray-based Gene Expression Profiling of Abdominal Aortic Aneurysm. *Eur J Vasc Endovasc Surg*. 2016;52(1):47-55. doi:10.1016/j.ejvs.2016.03.016
128. Jiang T, Si L, Jiang T, Si L. Identification of the molecular mechanisms associated with acute type A aortic dissection through bioinformatics methods. *Brazilian Journal of Medical and Biological Research*. 2019;52(11). doi:10.1590/1414-431x20198950
129. Lin S, Han X, Bi Y, Ju S, Gu L. Fluid-Structure Interaction in Abdominal Aortic Aneurysm: Effect of Modeling Techniques. *Biomed Res Int*. 2017;2017. doi:10.1155/2017/7023078
130. Sheidaei A, Hunley SC, Zeinali-Davarani S, Raguin LG, Baek S. Simulation of abdominal aortic aneurysm growth with updating hemodynamic loads using a realistic geometry. *Med Eng Phys*. 2011;33(1):80-88. doi:10.1016/j.medengphy.2010.09.012
131. Cornuz J, Sidoti Pinto C, Tevaearai H, Egger M. Risk factors for asymptomatic abdominal aortic aneurysm Systematic review and meta-analysis of population-based screening studies. *Eur J Public Health*. 2004;14(4):343-349. doi:10.1093/eurpub/14.4.343
132. Tanaka S, Fukumoto Y, Nochioka K, et al. Statins exert the pleiotropic effects through small GTP-binding protein dissociation stimulator upregulation with a

resultant Rac1 degradation. *Arterioscler Thromb Vasc Biol.* 2013;33(7):1591-1600.

doi:10.1161/ATVBAHA.112.300922

133. Yu D, Makkar G, Strickland DK, et al. Myristoylated Alanine-Rich Protein Kinase Substrate (MARCKS) Regulates Small GTPase Rac1 and Cdc42 Activity and Is a Critical Mediator of Vascular Smooth Muscle Cell Migration in Intimal Hyperplasia Formation. *J Am Heart Assoc.* 2015;4(10):e002255.

doi:10.1161/JAHA.115.002255

134. Hosni JJ, Vinagre CG, Mady C, Maranhão RC. Lipolysis of emulsion models of triglyceride-rich lipoproteins is altered in male patients with abdominal aorta aneurysm. *Braz J Med Biol Res.* 2007;40(3):305-307. doi:10.1590/s0100-879x2007000300004

135. Kugo H, Tanaka H, Moriyama T, Zaima N. Pathological Implication of Adipocytes in AAA Development and the Rupture. *Ann Vasc Dis.* 2018;11(2):159-168.

doi:10.3400/avd.ra.17-00130

136. Police Sara B., Thatcher Sean E., Charnigo Richard, Daugherty Alan, Cassis Lisa A. Obesity Promotes Inflammation in Periaortic Adipose Tissue and Angiotensin II-Induced Abdominal Aortic Aneurysm Formation. *Arteriosclerosis, Thrombosis, and Vascular Biology.* 2009;29(10):1458-1464. doi:10.1161/ATVBAHA.109.192658

137. Lindqvist M, Hellström A, Henriksson AE. Abdominal aortic aneurysm and the association with serum levels of Homocysteine, vitamins B6, B12 and Folate. *Am J Cardiovasc Dis.* 2012;2(4):318-322.

138. Wiernicki I, Parafiniuk M, Kolasa-Wołoskiuk A, et al. Relationship between aortic wall oxidative stress/proteolytic enzyme expression and intraluminal thrombus thickness indicates a novel pathomechanism in the progression of human abdominal aortic aneurysm. *FASEB J.* 2019;33(1):885-895. doi:10.1096/fj.201800633R

139. Berger EA, Murphy PM, Farber JM. CHEMOKINE RECEPTORS AS HIV-1 CORECEPTORS: Roles in Viral Entry, Tropism, and Disease. *Annu Rev Immunol.* 1999;17(1):657-700. doi:10.1146/annurev.immunol.17.1.657

140. Kohlmeier JE, Reiley WW, Perona-Wright G, et al. Inflammatory chemokine receptors regulate CD8+ T cell contraction and memory generation following infection. *J Exp Med.* 2011;208(8):1621-1634. doi:10.1084/jem.20102110

141. Ghilardi G, Biondi ML, Battaglioli L, Zambon A, Guagnellini E, Scorza R. Genetic risk factor characterizes abdominal aortic aneurysm from arterial occlusive

- disease in human beings: CCR5 Delta 32 deletion. *J Vasc Surg.* 2004;40(5):995-1000. doi:10.1016/j.jvs.2004.08.014
142. Phillips EH, Lorch AH, Durkes AC, Goergen CJ. Early pathological characterization of murine dissecting abdominal aortic aneurysms. *APL Bioengineering.* 2018;2(4):046106. doi:10.1063/1.5053708
143. Grarup N, Moltke I, Andersen MK, et al. Loss-of-function variants in ADCY3 increase risk of obesity and type 2 diabetes. *Nat Genet.* 2018;50(2):172-174. doi:10.1038/s41588-017-0022-7
144. Chen Y, Gong YW, Zhou XQ, Xu HX, Yang L, Wu YY. [Association between single nucleotide polymorphism of adenylyl cyclase 3 and essential hypertension]. *Zhonghua Xin Xue Guan Bing Za Zhi.* 2016;44(7):594-599. doi:10.3760/cma.j.issn.0253-3758.2016.07.008
145. Jama A, Huang D, Alshudukhi AA, Chrast R, Ren H. Lipin1 is required for skeletal muscle development by regulating MEF2c and MyoD expression. *J Physiol (Lond).* 2019;597(3):889-901. doi:10.1113/JP276919
146. Koh J-H, Kim K-H, Park S-Y, Kim Y-W, Kim J-Y. PPAR δ Attenuates Alcohol-Mediated Insulin Resistance by Enhancing Fatty Acid-Induced Mitochondrial Uncoupling and Antioxidant Defense in Skeletal Muscle. *Front Physiol.* 2020;11:749. doi:10.3389/fphys.2020.00749
147. Stierwalt HD, Ehrlicher SE, Robinson MM, Newsom SA. Skeletal Muscle ACSL Isoforms Relate to Measures of Fat Metabolism in Humans. *Med Sci Sports Exerc.* Published online August 11, 2020. doi:10.1249/MSS.0000000000002487
148. Kim HW, Weintraub NL. Aortic aneurysm: in defense of the vascular smooth muscle cell. *Arterioscler Thromb Vasc Biol.* 2016;36(11):2138-2140. doi:10.1161/ATVBAHA.116.308356

7 LISTS OF FIGURES AND TABLES

7.1 List of figures

Figure 1. Molecular mechanisms of VEGF signaling in endothelial tip-stalk switch during angiogenesis.

Figure 2. A brief overview of weighted gene co-expression network analysis.

Figure 3. The blue light device from the top side (left) and the bottom side (right).

Figure 4. Schematic diagram of blue light power measurements.

Figure 5. Schematic diagram of black plates used for the experiments.

Figure 6. The principle of the assay using Grx1-roGFP3.

Figure 7. Flowchart of analysis in the study.

Figure 8. Changes in the cell viability of HUVECs following different blue light fluences.

Figure 9. Cell viability changes of HUVECs after different durations of blue light irradiation.

Figure 10. Changes in the cell proliferation of HUVECs following different blue light fluences.

Figure 11. Changes in the cell viability of HUVECs following irradiance over the fixed time point of 12 minutes of XTT assay at 24 hours after irradiation.

Figure 12. Dynamic ROS changes of HUVECs as determined with the redox sensor following blue light exposure to either low fluence ($10 \text{ mW/cm}^2 * 12 \text{ min}$) or high fluence ($40 \text{ mW/cm}^2 * 12 \text{ min}$).

Figure 13. Changes in the ROS levels in HUVECs following exposure to either low fluence ($10 \text{ mW/cm}^2 * 12 \text{ min}$) or high fluence ($40 \text{ mW/cm}^2 * 12 \text{ min}$) using the DCFH-DA assay after irradiation.

Figure 14. Apoptosis changes in HUVECs following exposure to either low fluence ($10 \text{ mW/cm}^2 * 12 \text{ min}$) or high fluence ($40 \text{ mW/cm}^2 * 12 \text{ min}$) after irradiation using flow cytometer.

Figure 15. Cell migration determined by the scratch assay following exposure to either low fluence ($10 \text{ mW/cm}^2 * 12 \text{ min}$) or high fluence ($40 \text{ mW/cm}^2 * 12 \text{ min}$) after blue light irradiation.

Figure 16. Cell migration determined by the trans-well assay following exposure to either low fluence (10 mW/cm² * 12 min) or high fluence (40 mW/cm² * 12 min) after blue light irradiation.

Figure 17. Blue light affects tube formation and sprouting in HUVECs.

Figure 18. Principal component analysis (PCA) of RNA-seq data from HUVECs in non-irradiated control, low fluence (10 mW/cm² * 12 min) and high fluence (40 mW/cm² * 12 min) treatment group.

Figure 19. KEGG pathway enrichment analysis of low fluence (10 mW/cm² * 12 min) versus the non-irradiated control group.

Figure 20. KEGG pathway enrichment analysis of high fluence (40 mW/cm² * 12 min) versus the non-irradiated control group.

Figure 21. Gene set enrichment analysis of the interested pathways.

Figure 22. qPCR validation of genes in the interested pathways.

Figure 23. Construction of gene co-expression network by WGCNA.

Figure 24. Identification of the key modules associated with AAA progression.

Figure 25. Gene ontology enrichment analysis of key modules of AAA progression.

Figure 26. KEGG pathway enrichment analysis of key modules of AAA progression.

Figure 27. Validation of gene expression from hub genes in mouse dataset GSE12591.

Figure 28. Gene-drug interaction prediction of key genes.

7.2 List of tables

Table 1. Irradiation parameters were used in the study.

Table 2. Preparation of the amplifying hydrogel solution (AHS).

Table 3. Information of primer used in the study.

Table 4. The number of significantly differentially expressed (either up-and down-regulated genes) in HUVECs following blue light treatment with low fluence (10 mW/cm² * 12 min) and high fluence (40 mW/cm² * 12 min) compared with non-irradiated control.

Table 5. The number of differentially expressed KEGG pathways in HUVECs treated with low fluence (10 mW/cm² * 12 min) and high fluence (40 mW/cm² * 12 min) compared with non-irradiated controls.

Table 6. Number of the most affected KEGG pathways in HUVECs treated with low fluence ($10 \text{ mW/cm}^2 * 12 \text{ min}$) and high fluence ($40 \text{ mW/cm}^2 * 12 \text{ min}$) compared with non-irradiated control.

Table 7. Top 10 ranked genes in key modules with the MCC method in cytoHubba.

Table 8. Significantly expressed hub genes in human AAA datasets.

Table 9. Potential target agents identified based on drug-gene interaction in DGIdb database.

8 CURRICULUM VITAE

PERSONAL INFORMATION

Name: Kejia Kan
Date of birth: 29. 04.1990
Place of birth: Changshu, Jiangsu Province, China
Marital status: Married
Father: Lianghua Kan
Mother: Zhengying Gu

EDUCATION

Oct.2017-Present
M.D. Student (Dr.med.)
Department of Surgery, University Medical Center Mannheim,
Medical Faculty Mannheim, Heidelberg University,
Mannheim, Germany
Doctor Thesis: Influence of blue light irradiation on endothelial
cells and weighted gene co-expression network analysis in the
development of abdominal aortic aneurysm

Sept.2014-Jul.2017
Master's Degree of Medicine
Department of Vascular Surgery, Renji Hospital, Shanghai Jiao
Tong University School of Medicine,
Shanghai, China
Master Thesis: Study of the docking protein gab1 in the
regulation of vascular smooth muscle cell autophagy in
atherosclerosis

Sept.2009-Jul.2014
Bachelor's Degree of Medicine
Chongqing Medical University School of Medicine,
Chongqing, China

SCHOLARSHIP

M.D. scholarship from China Scholarship Council (CSC)

PUBLICATIONS

First authorship

1. **Ke-Jia Kan**, Feng Guo, Lei Zhu, Prama Pallavi, Martin Sigl, Michael Keese. Weighted Gene Co-Expression Network Analysis Reveals Key Genes and Potential Drugs in Abdominal Aortic Aneurysm. *Biomedicines*. 2021 May; 9(5): 546.

Co-authorship

1. Lei Zhu, **Ke-Jia Kan**, Johanna L Grün, Barbara Hissa, Cui Yang, Balázs Györffy, Sonja Loges, Christoph Reißfelder, Sebastian Schölch. GAS2L1 Is a Potential Biomarker of Circulating Tumor Cells in Pancreatic Cancer. *Cancers (Basel)*. 2020 Dec 15;12(12):3774.
2. Meng Ye, Xiang-Jiang Guo, **Ke-Jia Kan**, Qi-Hong Ni, Jia-Quan Chen, Han Wang, Xin Qian, Guan-Hua Xue, Hao-Yu Deng, Lan Zhang. Loss of GRB2 associated binding protein 1 in arteriosclerosis obliterans promotes host autophagy. *Chin Med J (Engl)*. 2020 Dec 8;134(1):73-80.

9 ACKNOWLEDGEMENT

First of all, I would like to thank Prof. Michael Keese for his supervision, support and all the knowledge that I have gained during this period. I thank him and Prof. Norbert Gretz for giving me the opportunity to work on this interesting project in collaboration with the Urgo Research team in France.

Secondly, I would like to thank Dr. Prama Pallavi for her inspiring advice, suggestions as well as comments and moreover her constant support throughout the whole project.

Furthermore, I am very grateful for all the experiences I gained as a member of the surgery lab in Mannheim. It was a pleasure to work with all the partners involved. I would like to take the opportunity to thank Prof. Sebastian Schölch and Prof. Nuh Rahbari for providing an excellent experimental platform. I also thank Marzena Knyssok-Sypniewski and Silke Deiters for their assistance in daily lab work. Besides, I would like to thank Dr. Carsten Sticht and Carolina De La Torre for their support in RNA sequencing.

Particularly, China Scholarship Council (CSC) is gratefully acknowledged for supporting my study in Germany.

Last but not least, I want to express my gratitude to my parents and my wife. Thank you for your constant support and patience. All my successes are also yours.